Differentiating the roles of proteins and polysomes in nucleoid size homeostasis in Escherichia coli

Mu-Hung Chang[1], Maxim O. Lavrentovich*[1,2], and Jaan Männik*[1]

[1]Department of Physics and Astronomy, The University of Tennessee, Knoxville, TN 37996, USA
[2]Department of Earth, Environment, and Physics, Worcester State University, Worcester, MA 01602, USA

Correspondence: mlavrent@utk.edu, jmannik@utk.edu

ABSTRACT A defining feature of the bacterial cytosolic interior is a distinct membrane-less organelle, the nucleoid, that contains the chromosomal DNA. Although increasing experimental evidence indicates that macromolecular crowding is the dominant mechanism for nucleoid formation, it has remained unclear which crowders control nucleoid volume. It is commonly assumed that polyribosomes play a dominant role, yet the volume fraction of soluble proteins in the cytosol is comparable to that of polyribosomes. Here, we develop a free energy-based model for the cytosolic interior of a bacterial cell to distinguish contributions arising from polyribosomes and cytosolic proteins in nucleoid volume control. The parameters of the model are determined from the existing experimental data. We show that while the polysomes establish the existence of the nucleoid as a distinct phase, the proteins control the nucleoid volume in physiologically relevant conditions. Our model explains experimental findings in *Escherichia coli* that the nucleoid compaction curves in osmotic shock measurements do not depend on cell growth rate and that dissociation of polysomes in slow growth rates does not lead to significant nucleoid expansion, while the nucleoid phase disappears in fastest growth rates. Furthermore, the model predicts a cross-over in the exclusion of crowders by their linear dimensions from the nucleoid phase: Below the cross-over of 30—50 nm, the concentration of crowders in the nucleoid phase decreases linearly as a function of the crowder diameter, while decreasing exponentially above the cross-over size. Our work points to the possibility that bacterial cells maintain nucleoid size and protein concentration homeostasis via feedback in which protein concentration controls nucleoid dimensions and the nucleoid dimensions control protein synthesis rate.

STATEMENT OF SIGNIFICANCE Bacterial chromosomal DNA is compacted into a membrane-less organelle called the nucleoid. DNA compaction can be expected to affect DNA replication, segregation, and, via transcription, most cellular processes. Although increasing evidence indicates that macromolecular crowding is responsible for the phase separation of the nucleoid from the remaining cytosol, the specific roles of different crowders remain poorly understood. We develop a free energy-based model of the bacterial cell interior to distinguish contributions arising from polysomes and proteins. Our model shows that while the polysomes establish the existence of a distinct nucleoid phase, the proteins control the phase volume in physiologically relevant conditions. Our work points to the possibility that bacterial cells maintain simultaneous nucleoid size and protein concentration homeostasis.

INTRODUCTION

All living cells organize their key biological processes in space to properly function and reproduce (1). A notable example is the organization of chromosomal DNA (2,3). In interphase eukaryotic cells, chromosomal DNA is confined by the nuclear membrane, and individual chromosomes occupy well-defined territories within the nucleus (4). Bacteria and archaea lack a nucleus, yet prokaryotic chromosomes do not spread over the whole cytosol, despite the considerable length of DNA. In *Escherichia coli* (*E. coli*), the chromosomal DNA is 1.6 mm long (4.6 Mb), but it occupies only about 50% of the available cytosolic volume in a typical cell that is about 3 μm long and less than 1 μm wide (5). This volume is referred to as the nucleoid. In growing *E. coli* the nucleoid size is found to be proportional to cell size during the cell cycle (6-8). However, the nucleoid size changes in response to growth conditions and varies significantly from one species to another (9). When released from the cell, the DNA expands to more than 100 times the cell volume (10,11). The significant compaction of chromosomes in bacterial cells can affect DNA replication, segregation, and transcription. Via the latter, the size of the nucleoid can influence most cellular processes. It is therefore of interest to understand the processes that compact the chromosomal DNA in a cell to a nucleoid.

Several factors contributing to the compaction of the nucleoid have been proposed, including nucleoid-associated proteins (NAPs), DNA supercoiling, and molecular crowding (2,12-14). The NAP, and, in particular, condensin-like MukBEF (15), have a significant effect on how the DNA is folded within the nucleoid (16). At high enough concentrations NAPs can compact DNA *in vitro* (17) and stationary phase cells *in vivo* (18). However, NAPs' activity appears not to significantly alter the global size of the nucleoid in log-phase cells. Deletion of genes coding for the NAPs one by one has only a minor effect on the size of the nucleoid in *E. coli* (7).

Similarly to NAPs, changing the supercoiling level of DNA in live cells appears also to have only a small effect on the size of the nucleoid (19). Notably, it has been observed that in virus-infected bacteria, where the host DNA becomes fragmented and torsionally relaxed, the cells still maintain compaction of chromosomal DNA (20). This finding can be explained by macromolecular crowders holding different DNA fragments together. Measurements in hyperosmotically shocked and mechanically squeezed *E. coli* cells also support the idea that macromolecular crowding plays a major role in nucleoid compaction (5,21). In these experiments, water was forced out from the cells, leading to a 3-fold decrease in nucleoid volume.

In mechanical squeezing experiments, such a decrease occurred at a 100 ms timescale (21). It is highly unlikely that the large-scale changes in supercoiling levels or DNA looping by MukBEF could have caused the nucleoid to compact at such short times. Instead, crowding-related compaction of the nucleoid resulting from the outflow of water and increased concentration of all macromolecular crowders offers a simple explanation for the observed rapid compression. *In vitro* measurements of nucleoids released from *E. coli* cells also strongly support that nucleoid compaction occurs via macromolecular crowding: Artificial crowding agents can compact the released DNA to the sizes observed in live cells (10,22).

The crowder-induced compaction of the nucleoid has been explained using equilibrium thermodynamics (free energy arguments) (23) and computer simulations (molecular dynamics) (24-28). The latter consider DNA as a flexible string of spherical beads and crowders as spherical particles. Both theoretical and modeling approaches consider only repulsive interactions and excluded volume effects. The repulsive interactions arise because DNA and most cytosolic macromolecules (crowders) are net negatively charged. All these previous works predict that DNA is compacted and that the cell's interior spontaneously separates into two liquid phases at sufficiently high crowder volume fraction. One of these phases, the nucleoid phase, contains the chromosomal DNA and is depleted of cytosolic macromolecules (Fig. 1a) (23,25,26). The second phase encompasses the remainder of the cytosol, lacks the chromosomal DNA, and is enriched in other macromolecules. We refer to this phase as the cytosolic phase (not to be confused with the whole cytosol). It is worth noting that the phase separation of bacterial cytosol arises due to repulsive interactions between DNA and the crowders. At the same time, the liquid-liquid phase separated organelles/condensates in eukaryotic cells (nucleolus, etc.) arise due to the attractive interactions between ribonucleic acids, mediated by specific positively charged proteins.

While macromolecular crowding compacts chromosomal DNA and is responsible for forming the nucleoid as a distinct organelle-like entity in the prokaryotic cell, the roles of different types of macromolecules remain unclear. The main macromolecules acting as cytosolic crowders in the bacterial cell are proteins, protein complexes, and polyribosomes (polysomes). Additionally, the 30S and 50S ribosome subunits contribute to the crowding, but to a smaller extent because most ribosomal RNA is involved in active translation as part of polysomes (>85%) in log-phase cells (29,30). tRNA species are also abundant, but their total excluded volume is much smaller than that of proteins and polysomes (5). Currently, most theoretical works assume that polysomes act as the main crowding agents for nucleoid compaction, and the contribution of the proteins can be neglected (25,31-34). The exception is the seminal work by Odijk, which concluded that cytosolic proteins have the dominant effect while the contribution

of polysomes can be neglected (23).

Our theoretical work aims to explain the existing experimental data (Yang *et al.* (5) and Xiang *et al.* (8)) on crowding effects on the *in vivo* nucleoid in wild type *Escherichia coli* cells. In the first part of the study, we investigate the contribution of polysomes and cytosolic soluble proteins on the compaction of the *E. coli* nucleoid using a free energy-based model. We compare the model predicions to experimental data by Yang *et al.* (5) where the variation of crowding levels on nucleoid dimensions were experimentally probed using osmotic shocks, mechanical perturbations, growth rate changes and dissociation of ribosomes. In contrast to previous modeling studies, where the effects of macromolecular crowding were addressed in a coarse-grained manner using Brownian dynamics simulations with spherical crowders (25,27,28,33,35), our model here explicitly accounts for the polymeric nature of polyribosomes. The model also considers supercoiling of chromosomal DNA and its effect on the excluded volume interactions. The advantage of the free energy approach is that, by sacrificing some of the microscopic details, the phenomenology of more macroscopic experimental measurements can be directly incorporated into the model parameters. Other modelling approaches, such as molecular dynamics, typically require a (usually simplified) microscopic model, such as a bead-and-spring representation of the DNA, with no obvious connection to experiments. So, to determine the unknown parameters of our model, we calibrate the free energy by fitting to experimental data obtained from *in vivo* measurements (5). Our results suggest that, in *E. coli* cells at physiological conditions, the nucleoid size depends more sensitively on the concentration of cytosolic proteins/protein complexes than on polysomes, even though the polysomes are more strongly excluded from the nucleoid. In other words, the polysomes establish the existence of the nucleoid phase, while the proteins control the overall volume of this phase. Our model can also explain a recent puzzling finding that the dissociation of polysomes to 30S and 50S subunits in slow growth rates has a minimal effect on nucleoid expansion (5). At the same time, our new experimental data shows that the nucleoid phase disappears at fast growth rates.

In the second part of the study, we explore how the nucleoid and cytosolic phases organize biological activity by partitioning differently-sized macromolecules. We may expect that larger macromolecules are excluded from the nucleoid. For example, experiments have shown that ribosomes (polysomes) are strongly excluded from the nucleoids (36-38). Consequently, translation appears to be concentrated in nucleoid-free regions in the cell. Recently, Xiang et al. measured the distribution of different-sized artificial particles (tracers) in *E. coli*, and developed a model based on scaling arguments to explain their results (8). The model predicted a characteristic mesh size of chromosomal DNA of about 50 nm and an

exclusion of all macromolecules larger than this size. Although the model gives a correct order of magnitude estimate for the excluded particle size, it cannot quantitatively predict the partial exclusion of different-sized macromolecules from the nucleoid. Here, our goal is to revisit the data by Xiang *et al* (8) using the free energy model mentioned above to investigate how macromolecules of different sizes are distributed between nucleoid and cytosolic phases. We find that the concentration of particles in the nucleoid region decreases approximately linearly when the diameter of the particle, a_t, is less than 30 nm and decreases exponentially for $a_t > 30$ nm.

The organization of the presentation is as follows: In the next section, we discuss our free energy model and the free energy minimization methods. In the Results section, we go through our model predictions and explanations for 1) the contribution of polysomes versus proteins in compacting the nucleoid, 2) the compaction properties of the nucleoid under different growth conditions, 3) the effects of polysome dissociation (rifampicin treatment) on nucleoid compaction, and 4) the partitioning of differently sized crowders between the cytosol and nucleoid regions. We conclude with a discussion of our results and possible future studies.

METHODS

We model the *E. coli* cell as a collection of proteins, polysomes, and chromosomal DNA contained in a cytosolic volume, V_{cell} (Fig. 1a,b). The notations for various quantities and their values are summarized in SI Table S1 and S2 and the main assumptions entering the model in SI Text (section "List of model assumptions"). We refer to both proteins and polysomes as crowders. For simplicity, we consider proteins to be monodisperse, hard spheres of diameter $a_p = 5$ nm. We treat polysomes as a "beads-on-a-string" polymer, where translating ribosomes are represented by the beads with a diameter $a_{\mathrm{ribo}} = 20$ nm attached to the corresponding mRNA, treated as a flexible (massless) string. We assume that there are, on average, ten translating ribosomes per mRNA ($N_{\mathrm{ribo}} = 10$) (31), although somewhat smaller average numbers were reported recently (39). This bead-on-a-string polymer has a characteristic radius of gyration R_g^{poly} which depends on the physical phase where the polysome resides and on the experimental conditions. For a given condition, we determine R_g^{poly} from minimizing the total free energy. We find R_g^{poly} only weakly depends on the experimental conditions, with a typical value $R_g^{\mathrm{poly}} \approx 35$ nm.

The total free energy of the above system can be written as a sum of self-energies of DNA, proteins and polysomes and their pairwise interaction terms:

$$F = F_0 + F_{\text{DNA}} + F_{\text{DNA-crowder}} + F_{\text{poly-protein}} + F_{\text{poly-poly}} \quad (1)$$

Here, F_0 denotes the free energy terms describing the corresponding crowder-only system (see SI Text for details) and F_{DNA} is the free energy of due to DNA self-interaction. The remaining three terms describe the interaction free energy between the three different molecular species. Below we describe the key terms in Eq. 1 in more detail while leaving the terms with a more conventional approach for the SI Text. In what follows, we write all free energies in units of k_BT unless otherwise specified.

DNA self-interaction

For the free energy F_{DNA} of the isolated DNA, we follow a power law formulation by Cunha *et al.* (10)

$$F_{\text{DNA}} = g\left(\frac{V_{\text{nuc,free}}}{V_{\text{nuc}}}\right)^{\alpha}. \quad (2)$$

Here, $V_{\text{nuc,free}}$ is the volume of the nucleoid (chromosome) in the absence of crowders and cellular confinement and V_{nuc} is the nucleoid volume inside the cell. It has been argued that g is proportional to the number of DNA crosslinks in the nucleoid (10), while the exponent α can be linked to the fractal dimension of DNA (see SI Text). Eq. 2 is a phenomenological model for DNA that is valid in the high compaction regime. An experiment with nucleoids liberated from *E. coli* cells has yielded the following estimates: $V_{\text{nuc,free}} \approx 27\,\mu\text{m}^3$, $g \approx 362$ and $\alpha \approx 1.34$ (10). Note that the presence of both g and $V_{\text{nuc,free}}$ overparameterizes Eq. 2. However, since these variables have been separately determined in the experiment, we choose to keep both. The values of $V_{\text{nuc,free}}$, g and α depend on the details of the interaction between DNA segments via DNA binding proteins such as MukBEF (condensin analog), H-NS and others (14). These interactions become perturbed upon the liberation of nucleoids from the cells as these proteins dissociate from the DNA. We, therefore, treat g and α as adjustable model parameters whose values we determine from fitting the model to experimental data (5), as will be explained below.

DNA-crowder interaction

We describe DNA-crowder interaction via the first-order virial coefficient B, representing the excluded volume between DNA and a crowder. We use a separate estimation of B for proteins and polysomes. For the excluded volume between DNA and proteins, $B_{\text{DNA-protein}}$, DNA supercoiling has a minor effect because proteins can diffuse into the supercoiled segments (Fig. 1b). The proteins are thus only excluded from the

cylindrical volume of the DNA double helix, with a diameter $d_{\mathrm{DNA}} \approx 2\ \mathrm{nm}$. Thus, the excluded volume interaction between DNA and proteins reads

$$B_{\text{DNA-protein}} = \frac{1}{4}\pi L_{\mathrm{DNA}}\left(d_{\mathrm{DNA}} + a_p\right)^2, \tag{3}$$

where L_{DNA} is the length of DNA. For a single fully replicated chromosome in *E. coli*, $L_{\mathrm{DNA}} = 1.6$ mm.

We must consider DNA supercoiling for the excluded volume between DNA and polysomes because the polysomes are too large to enter the supercoiled segments. To estimate the corresponding excluded volume, we represent a supercoiled segment of DNA as a cylinder (Fig. 1b) with a diameter $d_s = P\cos\delta$, where δ is the superhelical pitch angle, which has been reported around 52° (40), and $P \approx 50$ nm is the persistence length of the dsDNA (40). The number of these superhelical segments, N_s, was reported to be around 6700 (31,34). Assuming all chromosomal DNA forms a uniformly supercoiled structure, we write the excluded volume between DNA and polysomes as

$$B_{\text{DNA-poly}} = \frac{\pi}{8}\sin(\delta)\, L_{\mathrm{DNA}}\left(d_s + a_{\mathrm{poly}}\right)^2 + N_s\frac{\pi}{6}\left(d_s + a_{\mathrm{poly}}\right)^3, \tag{4}$$

where $a_{\mathrm{poly}} \equiv 2R_g^{\mathrm{poly}}$ is the effective polysome diameter, which can be calculated from the radius of the gyration value R_g^{poly} determined via free energy minimization. In Eq. 4, the first term describes the excluded volume interaction between the cylindrical part of the superhelical segments and the larger crowders. The second term is the interaction between the end caps of the superhelical segments and polysomes, as illustrated in Fig. 1b. We also consider other macromolecules whose size falls between proteins and polysomes. To treat these species, we use an interpolation formula between Eq. 3 and 4, as explained in detail in the SI Text.

Polysome-polysome interaction

To capture the interaction between polysomes, we use the results from the theory of polymer solutions. For a polymer in a good solvent, the osmotic pressure is well-approximated by combining the limiting behaviors in dilute and semidilute regimes (41). The two regimes are separated by an overlap volume fraction ϕ_{ov} defined as $\phi_{\mathrm{ov}} \equiv N_{\mathrm{ribo}} b^3 / \left(R_g^{\mathrm{poly}}\right)^3$, where b is the size of a single monomer (Kuhn length) and R_g^{poly} is the radius of gyration of the polysome. We take the diameter of the ribosome, $a_{\mathrm{ribo}} = 20$ nm, as the Kuhn length for polysomes, thereby assuming the mRNA connecting the ribosomes is highly flexible with a persistence length in 1-1.5 nm range (42). The resulting polysome osmotic pressure, extrapolating between the dilute and semidilute regimes (43), is given by

$$\Pi = \frac{n_{\text{poly}}}{V}\left[1 + \left(\frac{\phi_{\text{poly}}}{0.69\phi_{\text{ov}}}\right)^{1.309}\right], \quad (5)$$

where n_{poly} is the number of polysomes and V is the volume of the corresponding phase (nucleoid or cytosol). The value of the exponent, 1.309, follows from a renormalization group calculation (44). The free energy contribution due to polysome-polysome interaction from this osmotic pressure (see SI text for the derivation) is

$$F_{\text{poly-poly}} = \frac{n_{\text{poly}}}{1.309}\left(\frac{\phi_{\text{poly}}}{0.69\phi_{\text{ov}}}\right)^{1.309}. \quad (6)$$

Eq. 6 describes the non-ideal nature of the polysome mixture and is analogous to the Carnahan-Starling term of a hard sphere mixture that we use to describe protein-protein interactions (see SI text).

Minimizing the total free energy and determining model parameters

At a high enough crowder concentration, the total free energy in Eq. 1 exhibits phase separation, with a heterogeneous mixture yielding an overall lower free energy than a homogeneous one. Let us consider the phase-separated state in more detail. Assuming there is no additional cost to forming interfaces, the total free energy of the cell in the de-mixed state is the sum of free energies of each phase: $F_{\text{demix}} = F_{\text{nuc}} + F_{\text{cyto}}$. The free energy of the nucleoid F_{nuc} is given by Eq. 1, while the free energy for the cytosol phase F_{cyto} is given by the same equation but without the DNA self-interaction and DNA-crowder interaction terms. We find a free energy minimum with respect to the volume of the nucleoid phase, V_{nuc}, the numbers of each crowder species in each phase ($n_{\text{nuc}}^{\text{protein}}$, $\text{n}_{\text{nuc}}^{\text{poly}}$), and the radius of gyration of the polysomes (R_g^{poly}). To find these values, we minimize the total free energy F_{demix} using a simplex (Nelder-Mead) algorithm in the Python Scipy optimization library (45) (See SI text for detail).

The experimental uncertainties for several parameters entering the expression of the total free energy are considerable. These quantities include g and α in Eq. 2, along with the total numbers of ribosomes (polysomes) n_{poly} and proteins n_{proteins}. We determine the values of these parameters from least squares-fitting of the model to the experimental data from (5) (Fig. 1c). The experimental data originates from osmotic shock measurements of *E. coli* cells that determine the relative change of the nucleoid volume as a function of the relative change of crowder concentration. We refer to these curves as the nucleoid

compaction curves. The nucleoid volume in these curves is normalized by the volume of the nucleoid in unshocked cells, $V_{\mathrm{nuc},0}$, which we also refer to as the nucleoid volume at physiological condition. The concentration of crowders in these curves is normalized by the concentration of crowders in their unperturbed (physiological) condition, C_0. The normalized change in the concentration of crowders species i, $C_i/C_{i,0}$, is the same for all crowder species (i.e., $C_i/C_{i,0} = C/C_0$) because all changes in concentration in the experiments arise from the change in the total cell volume (with total macromolecule numbers fixed), i.e., $C/C_0 = V_{\mathrm{cell},0}/V_{\mathrm{cell}}$.

We again use the Nelder-Mead algorithm to fit the model parameters g, α, n_{poly}, and n_{protein} to experimentally-determined compaction curves via the least square method. The best-fit values we find are $g = 145$, $\alpha = 0.85$, $n_{\mathrm{poly}} = 600$ and $n_{\mathrm{protein}} = 2.3 \times 10^5$. The theoretical compaction curve differs from the data at higher concentration values $C/C_0 > 1.4$. This is expected for two reasons: First, the free energy approach assumes relatively dilute crowding conditions, which may not be valid at such high concentrations. Second, experimental determination of the nucleoid volume at high crowder concentrations is prone to systematic errors because the linear dimensions of the nucleoid approach the resolution limit of the microscope. Nevertheless, we find good agreement between our theory and the experimental curve over a wide range of concentrations. The values for g and α from the fit are both smaller than the values found previously from *in vitro* data ($g = 362$ and $\alpha = 1.34$ (10)). These g and α values from *in vitro* data give a poor fit to *in vivo* measurements (SI Fig. S1a). The smaller values of g and α for the *in vivo* conditions may arise from a different ionic environment (only monovalent salts were present in (10)), use of lysosome to liberate nucleoids (lysosome later binds to DNA after liberation (46)) or some other difference between *in vivo* and *in vitro* environments. The total number of polysomes $n_{\mathrm{poly}} = 600$ is in reasonable agreement with previous estimates (29,47). The total number of soluble proteins in the cytosol $n_{\mathrm{protein}} = 2.3 \times 10^5$ may appear lower than the typical estimates of few times 10^6 although more than an order of magnitude lower and higher estimates have been also reported (47). However, only fraction of the total proteins, which has been estimated to be in the range 20-40% (5), count as cytosolic crowders. Ribosomal proteins, proteins that bind to DNA including majority of RNA polymerazes and all the proteins associated with the cell envelopes do not count in our model as soluble cytosolic proteins. Furthermore, the estimates for protein numbers are drawn based fast growing cells while the fitting here is to data from slow growth where cell volumes and proteins numbers are about factor 2 smaller than in slow growth (Fig. S6a). In that light of

these considerations, $n_{\mathrm{protein}} = 2.3 \times 10^5$ is within a reasonable range. However, this number should not be interpreted beyond the scope of the current model because it depends on the chosen diameter of the typical protein, which is fixed to $a_p = 5$ nm in this study.

Analysis of nucleoid expansion in rifampicin-treated *E. coli* in EZ-Rich medium

While the remainder of the experimental data used to compare the model originates from previously published measurements (5,8), the effect of rifampicin treatment in EZ-Rich media has not been published. The measurement used *E. coli* MG1655 derivative strain JM57 as described in (5). The analysis protocol also follows the same work (5).

RESULTS

Soluble proteins control the nucleoid dimensions in physiological conditions while ribosomes establish the nucleoid phase.

Our first goal is to understand the relative contribution of polysomes and proteins to the compaction of the nucleoid. To that end, we consider a hypothetical cell whose volume is fixed but where the numbers of crowders can be varied. We will consider a variation that holds the number ratio of polysomes to proteins in the cell, $n_{\mathrm{poly}}/n_{\mathrm{protein}}$ (or concentration ratio), fixed. While such variation has not been experimentally measured, it allows us to describe key properties of the system in simple terms. We will discuss the effect of varying protein and polysome numbers to experimentally measured compaction curves in the next section.

To find how the nucleoid volume and the concentration of polysomes and proteins in the nucleoid phase vary as a function of the total concentration of polysomes and proteins in the cell we minimize the free energy, using the best-fit values for the parameters g and α from the previous section. We find the mixed state, where the nucleoid fills the whole cell volume, occurs only at dilute overall concentrations of crowders: $n_c/n_{c_0} = C/C_0 \approx 10^{-2}$ as shown in the inset of Fig. 2a. Here, n_c stands for either n_{poly} or n_{protein} and n_{c_0} is the corresponding value at physiological growth conditions. Increasing the number of crowders above $n_c/n_{c_0} \approx 10^{-2}$ favors the formation of the nucleoid phase. The formation of the nucleoid is accompanied by rapid depletion of polysomes from the nucleoid phase, which occurs over a small range of concentration ratios n_c/n_{c_0} (Fig. 2a, inset). The nearly discontinuous change in polysome concentration in the nucleoid is reminiscent of a first-order phase change.

The DNA and the polysomes are effectively immiscible to each other in the phase-separated regime. As a result of this immiscibility, the nucleoid volume decreases as more and more polysomes are added to the cell (moving from left to the right in Fig. 2a). At physiological concentrations ($n_c/n_{c_0} \approx 1$), the nucleoid volume begins to decrease more rapidly as more crowders are added to the cell. This decrease is accompanied by the onset of the depletion of proteins from the nucleoid phase (Fig. 2a). The depletion slows down once the concentrations of proteins and polyribosomes exceed their physiological values by about 25%. At this concentration, the depletion of proteins from the nucleoid is about 50%.

To delineate the contribution of proteins and polysomes to nucleoid compaction, we consider hypothetical cells where only polysomes (Fig. 2b) or only proteins (Fig. 2c) are present. For a cell with only polysomes, the nucleoid volume for the low crowder concentration changes the same way as for the cell where both polysomes and proteins are present (Fig. 2b). For low crowder concentrations ($n_c/n_{c_0} < 0.5$) polysomes thus solely determine the volume of the nucleoid (a shaded region in Fig. 2b). Conversely, for a cell with only protein crowders, the mixed state is conspicuously present and only vanishes for $n_c/n_{c_0} > 1.4$ (Fig. 2c). The mixed state collapses abruptly to a highly compacted nucleoid state with $V_{\mathrm{nuc}} = 0.2V_{\mathrm{cell}}$. After an abrupt decrease, the nucleoid volume further gradually decreases as the total number of proteins in the cell increases (Fig. 2c). For $n_c/n_{c_0} \gtrsim 1.5$, the change of nucleoid volume in the cell with only proteins is almost the same as in the cell where both crowder species were present (a shaded region in Fig. 2c), which indicates that proteins play a dominant role in compacting the nucleoid in the high crowder concentration regime.

These comparisons thus show that polysomes determine the nucleoid volume at low crowder concentrations, while at high crowder concentrations, the contribution from proteins dominates. The 3-fold compaction of the nucleoid in osmotic shock measurements results from protein crowders leaving the nucleoid phase. In other words, the polysomes are responsible for the initial compaction and phase separation of the nucleoid from the cytosol phase, while the proteins determine the homeostatic size of the nucleoid near the physiologically most relevant range of crowder concentrations.

The previous discussion explained qualitatively the contributions of proteins and polysomes on the nucleoid volume. To quantify these contributions, we investigated the differences in partial osmotic pressures of polysomes $\Delta\Pi_{\mathrm{poly}}$ and proteins $\Delta\Pi_{\mathrm{protein}}$ between the nucleoid and cytosolic phases. The usual definition of partial pressure, which is the pressure when only a single species is present, is not informative for our system because of strong interactions between species. Instead, we defined these pressures when other

species are still present (see SI Text for details). To avoid ambiguity arising from the interaction term between polysome and protein crowders, we assigned equal contributions from this term to both polysome and protein partial pressures. Using this definition, $\Delta\Pi_{\mathrm{poly}} + \Delta\Pi_{\mathrm{protein}}$, balances the bulk stress in the DNA coil due to its self-energy ($\tau_{\mathrm{DNA}} \equiv -\frac{\partial F_{\mathrm{DNA}}}{\partial V_{\mathrm{nuc}}} = \alpha g V_{\mathrm{nuc,free}}^{\alpha}/V_{\mathrm{nuc}}^{\alpha+1}$). The analysis shows (Fig. 2d) that the partial pressure of polysomes increases linearly for $n_c/n_{c,0} < 0.9$ and then reaches a plateau where $\Delta\Pi_{\mathrm{poly}} \approx 125$ Pa. In this regime, the contribution from proteins is small and negative. Negative values for $\Delta\Pi_{\mathrm{protein}}$ indicate that crowding due to protein crowders (in the presence of polysomes) favors expansion of the nucleoid instead of compaction. However, at about the same point where the osmotic pressure of the polysomes plateaus ($n_c/n_{c,0} \approx 0.9$), $\Delta\Pi_{\mathrm{protein}}$ starts to increase. At $n_c/n_{c,0} \approx 1.25$, $\Delta\Pi_{\mathrm{protein}}$ becomes equal to the contribution from polysomes and exceeds it after that (Fig. 2d). Despite significant compaction of the nucleoid at $n_c/n_{c,0} \approx 1.25$, all the pressures/stresses remain in this range on the order of 100 Pa. These pressures are significantly less than the osmotic pressure difference between the cell interior and exterior (estimated to be $200 - 300$ kPa (48)).

To conclude, the quantitative analysis of protein and polysome contributions shows that, at the physiological concentrations ($n_c/n_{c0} = 1$), the contribution of the partial osmotic pressure of polysomes exceeds the partial osmotic pressure of proteins. Consequently, polysomes are the main source of compaction of nucleoids. However, at $n_c/n_{c0} \approx 1$, $\Delta\Pi_{\mathrm{poly}}$ is effectively constant while $\Delta\Pi_{\mathrm{protein}}$ increases rapidly as the concentration of crowders increases. The latter finding further confirms that the proteins determine the variation of the nucleoid size near the physiologically most relevant range of crowder concentrations.

Scaling properties of the nucleoid compaction curves explain experimental data at different growth rates

We will next characterize what effect the variations of protein and polysome numbers have on the experimentally accessible portion of the nucleoid compaction curves. The compaction curves differ from those in the previous section (Fig. 2), where the number of crowders changes at fixed cell volume. Here, the volume of the cell changes at a set number of crowders. We find that variation of the protein number around the value found from the fit to the experimental data ($n_{\mathrm{protein}} = 2.3 \cdot 10^5$) while holding the polysome number fixed leads to a change in the shape of the compaction curve (Fig. 3a, S2). At low protein numbers, a knee-like bend is present at $C/C_0 = 1.0 - 1.2$, which gradually disappears as the protein

number increases. Contrary to protein number changes, a 2.5-fold variation in the polysome number changes do not affect the compaction curve (Fig. 3b). This invariance of the compaction curve with respect to polysome number explains the unexpected experimental finding from Ref. (5) that the nucleoid compaction curves were effectively the same in two different growth media where the growth rate of the cells differed by about a factor of two (SI Table S3). The finding was unexpected because the polysome concentration has been determined to be also approximately two-fold different in these two growth conditions (30) (see also SI Fig. S6b), while the protein concentration has been estimated to be almost the same (39). As Fig. 3b shows, the 2.5-fold variation in polysome concentration has effectively no effect on the nucleoid volume when the latter is scaled by $V_{\mathrm{nuc},0}$. This result thus explains the experimentally observed insensitivity of the nucleoid compaction curves to changes in cell growth rates and polysome concentrations.

We also investigated the scaling properties of $V_{\mathrm{nuc}}/V_{\mathrm{cell}}$ vs C/C_0 curves for the case when cell volume is fixed. Molecular dynamics modeling has shown that the poly-dispersity of crowders does not change the shape of these curves when plotted against an appropriately scaled "crowding level" (5,35) defined as $\sum_i a_{c,i}^2\, C_{c,i}$, where i represents different crowder species (Fig. S3a). We did not find such collapse in our model (Fig. S3b) when both proteins and polysomes were present. There may be two reasons for this. First, in our model, the polysomes and proteins interact differently with supercoiled DNA (Eq. 4, 5). Conversely, the molecular dynamics simulations used in (35) consider the same Weeks-Chandler-Anderson potential between a monomer of the DNA chain and any kind of crowder species, varying only the crowder radius. We verified that this difference is significant by neglecting the supercoiling structure of the DNA by replacing the polysome-DNA interaction with an interaction between a hard sphere (the polysome) and a hard cylinder (the DNA strand). In this case, we found that the curves of various crowder compositions acquired a similar shape but there was no collapse (Fig. S3c). A second factor likely influencing the collapse is our phenomenological scaling form for the DNA self-interaction, which is not necessarily obeyed by the string-and-beads DNA model, except at very high compressions.

The effect of polysome dissociation on the compaction of the nucleoid at different growth rates

Breaking up polysomes into 30S and 50S ribosome subunits by rifampicin (Rif) treatment (Fig. 4a) has been known to lead to the expansion of the nucleoid (8,49-51). A potential explanation for this expansion

has been that 30S and 50S subunits compact DNA less efficiently than polyribosomes. This prediction was confirmed by computer modeling (31). Interestingly, data from recent experiments indicated that nucleoid expansion is growth rate dependent, with relatively modest expansions at slower growth rates (5). We revisited these data, analyzing the expansion of the nucleoid with respect to cytosolic volume. In addition to the previously published data in slow and moderately fast growth rates, we considered a measurement at fast growth rates in EZ-Rich medium (Fig. 4b, SI Fig. S4). Unexpectedly, we found that the Rif treatment led to an expansion of the nucleoid throughout the whole cytosolic volume in the fast growth conditions, indicating the complete abolishment of the nucleoid phase. Such a response to Rif contrasts the one at slower growth rates where, based on quantitative data analysis, the nucleoid phase remains present (5,8). Note that the curve for $V_{\mathrm{nuc}}/V_{\mathrm{cell}}$ in Fig. 4b in fast growth rates does not reach 1, which may appear to contradict the conclusion about lacking nucleoid phase. The reason for $V_{\mathrm{nuc}}/V_{\mathrm{cell}} \approx 0.95 < 1.0$ is that, even in the mixed state, the DNA density near the plasma membrane drops due to the finite bending radius of DNA ($l_p \approx 50$ nm). Consistent with this assessment, the width of the nucleoid after the treatment remains about 40 nm smaller than the cytosolic width (SI Fig. S4b).

We shall now discuss what insights our model provides to help explain such pronounced growth-rate dependence of nucleoid expansion. To model the effect of rifampicin treatment, we replaced the polysome with the corresponding number of 30S and 50S ribosome subunits (a total of $2N_{\mathrm{ribo}} = 20$ subunits for each polysome), keeping the other parameters of the model unchanged. We assumed both ribosome subunits to be spherical particles of approximately the same diameter (~ 16 nm, see SI Text). Under such an assumption, the total volume of ribosome-associated crowders is roughly the same before and after the dissociation of polysomes. Comparing the experimentally measured nucleoid compaction curve in rifampicin-treated cells to the model predictions while considering only the polysome dissociation into subunits did not yield a good match (SI Fig. S5a). However, rifampicin treatment could alter the supercoiling level of DNA since rifampicin inhibits transcription, a key factor determining the supercoiling level (49,52). In our model, the change in supercoiling level can be expected to change factor g (Eq. 2), or equivalently $V_{\mathrm{nuc,\,free}}$. To find the g in rifampicin treated cells, we fit our theoretical model for the nucleoid compaction curves to the experimentally measured curves in Rif-treated cells (5), generating a new fit value $g = 200$ (SI Fig. S5b). This new value is larger than the value we calculated for untreated cells ($g = 145$), presumably because the treatment results in an expansion of the isolated nucleoid (larger $V_{\mathrm{nuc,\,free}}$) due to lower levels of DNA supercoiling.

To understand the growth rate dependence of nucleoid expansion under polysome dissociation, we needed to account for the growth-rate dependence of polysome and protein numbers, the amount of DNA in the cell, and the cell volume (for details, see SI Text). The available data for these quantities come from measurements at 37 °C, while the fitted data (Fig. 1c) is from measurements at 28 °C. The higher temperature is not expected to change these quantities (53), but temperature rise increases growth rates, μ. To use the existing experimental data, we matched the growth rates from 28 °C measurements (5) to those at 37 °C (SI Table S3). Since there is no experimental data available for the concentration of cytosolic protein crowders, we mapped out the relative dimensions of the nucleoid, $V_{\mathrm{nuc}}/V_{\mathrm{cell}}$, as a function of both protein crowder concentration and doubling time, $T_D = \ln(2)/\mu$ before and after Rif treatment (Fig. 4c, d, respectively). The model predicts the nucleoid phase to be present for all protein volume fractions and doubling times for the untreated cells (Fig. 4c). For the Rif treated cells, the resulting (phase) diagram is partitioned into two distinct regions: The nucleoid phase is present in the region of high protein volume fractions/concentrations and is absent at low volume fractions (Fig. 4d). The model thus predicts two distinct growth-rate related responses of the nucleoid to the dissociation of polysomes, consistent with the experimental observations.

The total protein concentration in *E. coli* cells has been found to slightly decrease with increasing growth rate (39). Based on the data in (39), we estimate the total protein concentration decreases by about 25% from the slow to fast growth condition of Fig. 4b. If the cytosolic protein volume fraction would decrease the same way, then the de-mixed state for the nucleoid would appear only for unrealistically short doubling times ($T_D < 15$ min) in our model. This discrepancy may arise from large uncertainties in the experimental growth rate dependencies (SI Text) that entered the calculation. However, it is also plausible that the concentration of cytosolic protein crowders decreases with the growth rate faster than the total concentration of the proteins in the cells. This is sensible because the cytosolic protein crowders are mostly enzymes involved in central metabolism. Cells achieve fast growth rates in high nutrient quality medium, where many of the enzymes for metabolism are not expressed because the enzymatic products are already present in the growth medium. Decreasing cytosolic crowder concentration at higher growth rates is also consistent with the notion that ribosome concentration increases proportionately to the growth rate. Since proteins contribute about half of the mass of the ribosomes (and polysomes) and the total protein is only weakly dependent on the growth rate, then it follows that protein concentration in other sectors (membrane proteins and soluble proteins that are not part of the ribosomes) needs to decrease more significantly as a function of growth rate. These arguments together thus suggest that the concentration of soluble cytosolic proteins that are not part of ribosomes decreases with the

increasing growth rate more significantly than the total protein concentration. In this scenario, the protein concentration (volume fraction) would follow the red-dashed arrow displayed in Fig. 4d when the growth rate increases. This line crosses from a mixed state to a de-mixed state at doubling times close to the one found from the experiments in the fast growth conditions (Fig. 4e). It is worth emphasizing that Rif treatment may introduce other effects beyond dissociation of polysomes that alter the size of the nucleoid. For example, inhibition of transcription is likely to alter supercoiling levels of chromosomal DNA. Nevertheless, the lack of the nucleoid phase in Rif-treated *E. coli* cells in fast growth rates can be explained by our model solely by dissociation of polysomes to ribosomal 30S and 50S subuinits and by assuming that the concentration of cytosolic protein crowders decreases with the increasing growth rate faster than the total protein concentration in the cell.

Partitioning of macromolecules between the nucleoid and cytosol phases based on their linear dimensions

Nucleoid compaction by macromolecular crowders is linked to the question of how macromolecules are distributed (partitioned) between the nucleoid and cytosolic phases. This distribution represents a key organizing principle of the bacterial interior, which typically lacks membrane-bound organelles. A recent study has addressed this question experimentally, following the distribution of differently-sized artificial particles within the *E. coli* cytosol (8). The experimental findings from this study were explained by arguing that the partitioning is determined by a characteristic mesh size of chromosomal DNA, as derived from a scaling approach. Particles smaller than the mesh size were postulated to be included in the nucleoid, while the larger ones were excluded. Our goal here is to find a quantitative distribution of particles by their sizes beyond this categorical estimate. To that end, we added additional spherical particles (tracers) to our model at dilute concentrations (maximal volume fraction $\phi_{max} \approx 0.002$) so that their presence did not perturb nucleoid volume. We then determined the distribution of these particles between the nucleoid and cytosolic phases as a function of the particle diameter a_t (see SI Text/Methods for details).

Our model predicts the concentration of the particles in the nucleoid phase to decrease monotonically as the diameter of tracer particles increases (Fig. 5a). According to the model, most proteins and protein complexes ($a_t = 1 - 10$ nm) distribute almost uniformly between the two phases at physiological conditions. For a particle with $a_t = 10$ nm, the depletion from the nucleoid phase is only 5%. For larger particles in the range $a_t = 10 - 25$ nm, the concentration of particles in the nucleoid phase decreases

approximately linearly with a_t. This range includes the 30S and 50S ribosomal subunits and 70S and 100S ribosomal particles. Our model predicts that free 30S and 50S subunits are ~ 40% excluded from the nucleoid, consistent with the qualitative conclusions made in the previous experimental study (51). Beyond this linear region, the concentration of tracers in the nucleoid phase shows an exponential decay with a_t (Fig. 5b). The cross-over to exponential decay occurs due to the interaction of tracer particles with DNA supercoils instead of single-stranded DNA. Particles with $a_t \geq 30$ nm are effectively entirely excluded from the nucleoid. This regime applies to polysomes. The model predicts their concentration in the nucleoid region to be only 10^{-4} of their total concentration. The cross-over region in our model approximately represents the effective mesh size of the earlier work. We find it to be about 30 nm, which is smaller than the 60 nm reported in (8).

The difference may be due to a difference in strains, as our estimate is based on parameters derived from the nucleoid compaction experiments of Ref. (5). Furthermore, it is difficult to directly compare the concentrations reported here to the average "exclusion score" calculated in Ref. (8). The latter includes contributions from particles from both phases rather than solely from the nucleoid phase as we assume in our calculations. Considering these uncertainties, our model is consistent with these experimental data and shows that the nucleoid phase strongly excludes polysomes. Our model also predicts that the exclusion effects of larger protein complexes and 30S and 50S particles from the nucleoid are not negligible. This effect could be functionally relevant in controlling translation.

DISCUSSION AND CONCLUSION

We investigated the compaction of the nucleoid and the spatial distribution of cellular components in *E. coli* cells based on an equilibrium free energy model. Unlike previous attempts to address the problem in a coarse-grained manner using Brownian dynamics simulations (25,27,28,33,35), our model is more specific in describing the molecular details of soluble proteins and polyribosomes, the dominant crowders in prokaryotic cells. Previous works have assumed that the dominant crowders species in the cell are polysomes while neglecting the crowding from proteins (25,31-34). Our model incorporates the polymeric nature of polysomes and the supercoiling of chromosomal DNA. We also extract the key parameters of the model from experimental data. The resulting model suggests that polysomes and cytosolic proteins are both needed to explain the experimentally determined compaction curves of the nucleoid under external hyperosmotic shock (5), with the largest changes in nucleoid volume coming from protein crowders leaving from the nucleoid volume. Protein crowders are effectively solely responsible for the

approximately 3-fold decrease in the nucleoid volume upon the highest osmotic shocks of about 1 Osm ($C/C_0 \gtrsim 1.4$ in Fig. 1c).

Although osmotic shocks are common natural occurrences for *E. coli* cells, it is relevant to understand how protein and polysome numbers control the volume of the nucleoid in unperturbed, steady-state conditions. Even in well-controlled growth environments, such as in chemostats or microfluidic devices, the concentrations of ribosomes and proteins vary from cell to cell. There are, as yet, no experimental data available on these fluctuations, but we consider the plausible range to be about ±20% relative to the mean value (based also on our preliminary data on ribosomes). Our model predicts that the variation of ribosome concentration in this range about its mean value causes only a 15% change in the nucleoid volume (Fig. 6). This variation is symmetric relative to the mean value. By contrast, variation of protein concentration in the same range causes an asymmetric 55% change. The depletion of proteins from their typical values has only a minor effect, while a 20% excess leads to about 50% compaction of the nucleoid from its physiological value. Fig. 6 thus further emphasizes the conclusion that proteins are the dominant species in controlling the dimension of the nucleoid in normal growth conditions.

It might not be a coincidence that the protein concentration is just below the level at which rapid compaction of nucleoid dimensions starts in steady-state growth conditions (Fig. 6). It is possible that transcriptional activity is increasingly suppressed as the dimensions of the nucleoids shrink. Suppression of transcriptional activity by nucleoid compaction suggests a feedback mechanism between nucleoid size and protein concentration that simultaneously maintains the volume of the nucleoid and protein concentration. In this putative scenario, excess expression of proteins in a cell leads to a more compacted nucleoid which then slows down protein expression. Once the protein expression decreases, the concentration of proteins decreases due to cell growth (dilution) which leads to a more expanded nucleoid and increased protein synthesis. It has been proposed that cells maintain crowding homeostasis by actively regulating the volume fraction of crowders in the cell (54). The scenario proposed here is one possible mechanism for maintaining this crowding homeostasis. Further experimental work linking global protein expression levels to nucleoid dimensions is needed to determine if this hypothetical feedback mechanism is present in *E. coli* and other bacteria. In such experiments, one could upregulate a concentration of soluble proteins (such as GFP) by expressing them from a high copy number plasmid while determining time-dependent response of the nucleoid volume to such changes.

Our model considers the cell's interior to be in equilibrium. In actuality, many energy-driven processes

are occurring in the cell, including DNA replication, gene transcription, and translation. The former two could significantly alter the level of nucleoid compaction. Given that our model can explain several experimental findings, the effects of replication and transcription can likely be effectively accounted for by the chosen form of DNA self-energy (Eq. 2) by adjusting parameters α, g and $V_{\mathrm{nuc,free}}$ in various environments/growth conditions, as we have done here. We found that g was the smallest for cells in physiological conditions ($g = 145$), intermediate for the Rif-treated cells ($g = 200$), and the largest for liberated nucleoids ($g = 362$ based on (10)). Increasing g in this series is equivalent to increasing $V_{\mathrm{nuc,free}}$ in Eq. 2. Decreasing the energy driven DNA processes appears thus to enlarge the intrinsic volume of the nucleoid. The larger intrinsic nucleoid volume could be caused by lower supercoil density. Most DNA transactions (transcription, replication, etc.) alter DNA supercoiling levels.

Like DNA, polysomes are also inherently dynamic and energy-driven entities. The lifetime of individual ribosomes in a polysome complex is 10-20 seconds (39). At this time scale, ribosomes leave mRNA after completing the synthesis of an average-sized protein. New ribosomes are also expected to assemble on the mRNA from their 30S and 50S subunits at about the same rate (39), so that there is an overall steady-state number of ribosomes on a given mRNA. Since the 30S and 50S subunits are not excluded from the nucleoid (Fig. 5a), polysomes can assemble within the nucleoid. Indeed, co-transcriptional translation is a well-described phenomenon in *E. coli* and other bacteria (55). Assembly of polysomes within the nucleoid and co-transcriptional translation have not been accounted for by our model, meaning that we likely underestimate the number of polysomes in the nucleoid phase. However, if the partitioning of other macromolecules between the nucleoid and cytosolic phases is more consistent with equilibrium, then this underestimation may not qualitatively affect our conclusions. The fraction of polysomes involved in co-transcriptional translation can be again taken into account by modifying the effective DNA self-energy (Eq. 2) and excluding their number from the total polysome number, n_{poly}. However, the polysomes involved in co-transcriptional translation may affect the results from our model in Rif-treated cells, where the effective number of subunits after the treatment could be higher than we estimate now ($10N_{\mathrm{poly}}$).

The effects of polysome dynamics and the ability of ribosome (subunits) to diffuse into the nucleoid were recently described by a kinetic model (34). The model was able to explain the positioning of two nucleoids at the cell's quarter positions and the splitting of a single nucleoid into two lobes in long filamentous *E. coli* cells. However, the model did not consider crowding effects arising from proteins, and it represented

DNA as a set of disjoint cylinders. Also, the assumption that the ribosome concentration in the filamentous cells remains unchanged compared to their value in normal cells may not have been justified (56). In the future, we plan on incorporating non-equilibrium effects arising from the dynamics of polysomes as in (34) with a more detailed description of supercoiled chromosomes and incorporation of protein crowders to find a more complete description for the dynamic interior of *E. coli*.

In summary, our model predicts that the increase in the concentration of soluble cytosolic proteins from their physiological value leads to significant compaction of the nucleoid volume. At the same time, although the presence of polysomes is needed for the formation of the nucleoid phase, the polysome concentration has a much smaller effect on nucleoid size. Growing cells maintain a remarkably constant nucleoid size to cell size ratio (9). It remains to be tested in future experiments if the nucleoid size homeostasis is achieved by a feedback mechanism whereby the nucleoid compaction downregulates protein synthesis.

AUTHOR CONTRIBUTIONS

JM and MOL designed the research. MC performed the modeling. All authors contributed to the writing of the paper.

ACKNOWLEDGMENTS

The authors thank Steve Abel, Chathuddasie Amarasinghe, Jaana Männik, Charlotte Pfeifer, and Conrad Woldringh for useful discussions and Da Yang for help in experiments. A part of this research was conducted at the Center for Nanophase Materials Sciences, which is sponsored at Oak Ridge National Laboratory by the Scientific User Facilities Division, Office of Basic Energy Sciences, U.S. Department of Energy. This work was supported in part by the US-Israel BSF research grant 2017004 (JM), by the National Institutes of Health award GM127413 (JM), NSF research grants MCB2313719 (JM, MOL) and by NSF MCB2219289 (MOL).

DECLARATION OF INTEREST

The authors declare no competing interests.

Figures

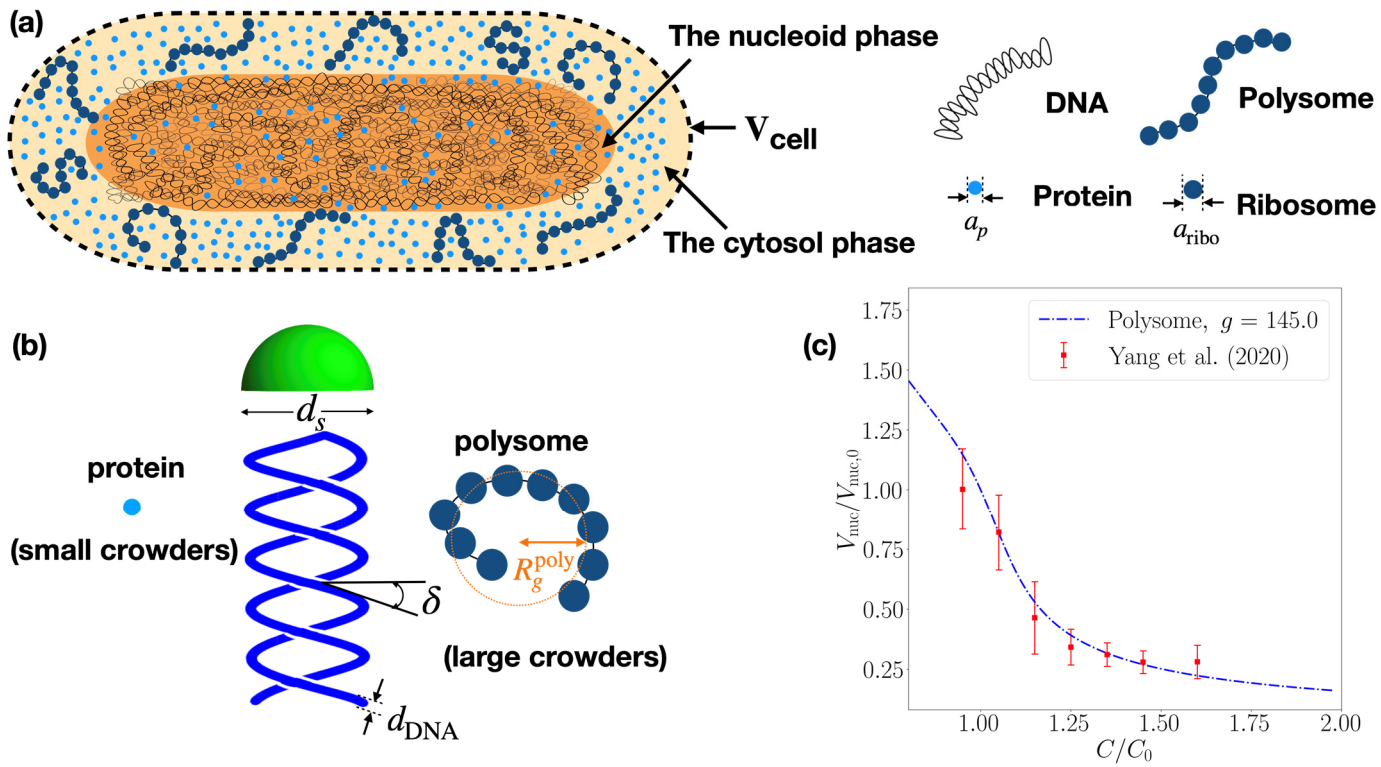

Figure 1: Defining the model. (a) A schematic for the cytosolic interior in *E. coli*. Supercoiled DNA occupies the nucleoid phase (dark brown), which phase-separates from the rest of the cytosol. The latter is referred to as the cytosol phase (light yellow). Here a cylindrical cell is depicted while the model neglects the cell shape. (b) Polysomes and proteins are the two main macromolecular crowder species in the cytosolic interior. The polysomes are modeled as a "beads on a string" polymer consisting of $N_{\text{ribo}} = 10$ ribosomes, each of diameter $a_{\text{ribo}} = 20$ nm. The cytosolic proteins are considered as hard sphere particles with diameter $a_p = 5$ nm. Polysomes due to their large effective radius, R_g^{poly}, cannot diffuse through DNA supercoils while proteins can. A DNA supercoil is modeled as helix with a diameter of d_s= 30 nm and the pitch angle $\delta = 52°$. (c) Fitting the experimental data on nucleoid volume vs crowder concentration from osmotic shock measurements (5) to the free energy model. The nucleoid volume and each crowder concentration is scaled by their respective values in not osmotically shocked cells. The best fit parameters for the model are $g \approx 145.0$, $\alpha \approx 0.85$, $n_{\text{poly},0} \approx 600$ and $n_{\text{protein},0} \approx 2.3 \times 10^5$. The reduced chi-squared of the fitting $\chi_r^2 \approx 13.6$.

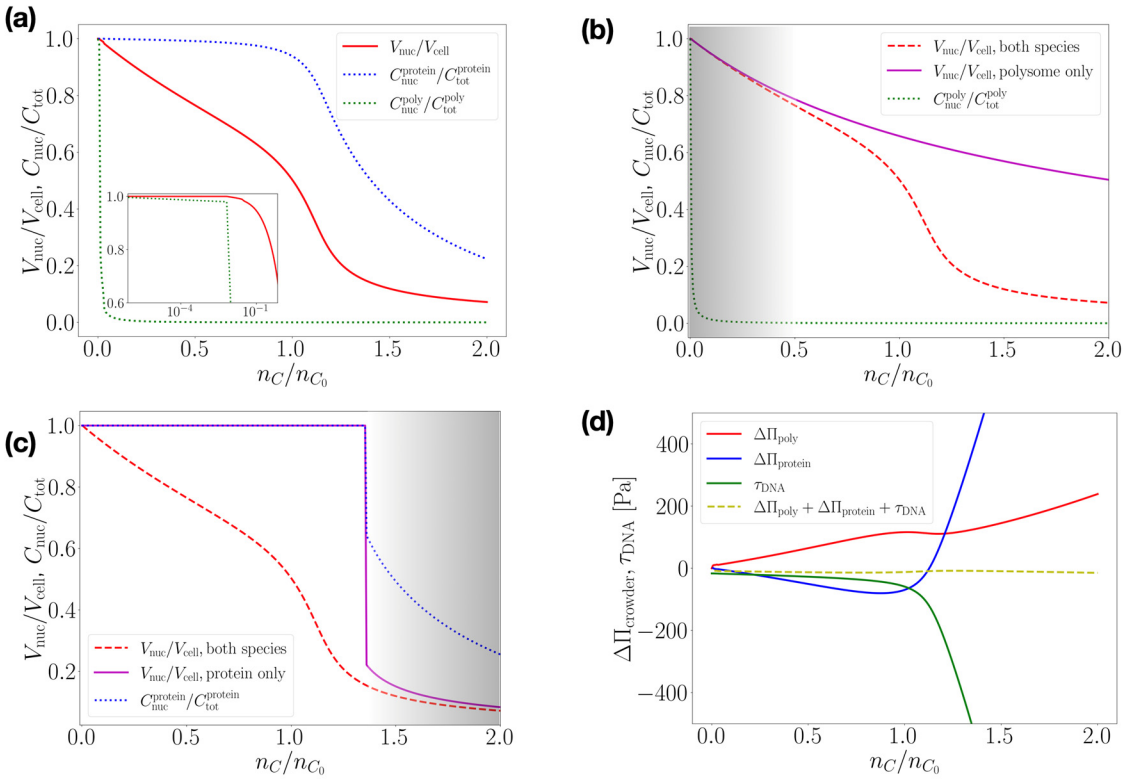

Figure 2: Differentiating contributions from proteins and polysomes to nucleoid compaction. (a) The nucleoid compaction curve (solid red line) and the relative crowder concentrations within the nucleoid phase $C_{\mathrm{nuc}}/C_{\mathrm{tot}}$ (blue and green dotted lines) as a function of number of crowders at fixed cell volume $V_{\mathrm{cell}} = 0.7\ \mu\mathrm{m}^3$. The best fit parameters from Fig. 1c are used. Here, n_c stands for either n_{poly} or n_{protein} and n_{c_0} is the corresponding value at normal growth conditions. The number of both macromolecular crowder species (proteins and polysomes) is proportional to each other throughout the curve. The inset shows the same data for the low crowder number region in semi-log scale. (b) The same curves when polysomes are the only crowder species (magenta solid and green dot lines, respectively). The red dashed line is the reference curve from panel (a), where both crowder species are present. The shading indicates a region where both compaction curves match. (c) The same curves when proteins are the only crowder species (magenta solid and blue dot lines, respectively). The shading indicates the region where contribution from proteins determines the shape of the overall compaction curve. (d) The differences in partial osmotic pressure of crowder species between the two phases ($\Delta\Pi_{\mathrm{poly}}$, $\Delta\Pi_{\mathrm{protein}}$) and the bulk stress in DNA coil (τ_{DNA}) as a function of n_c/n_{c_0}. The yellow dashed line represents the sum of the three solid curves in the plot. Temperature is assumed to be 37 °C.

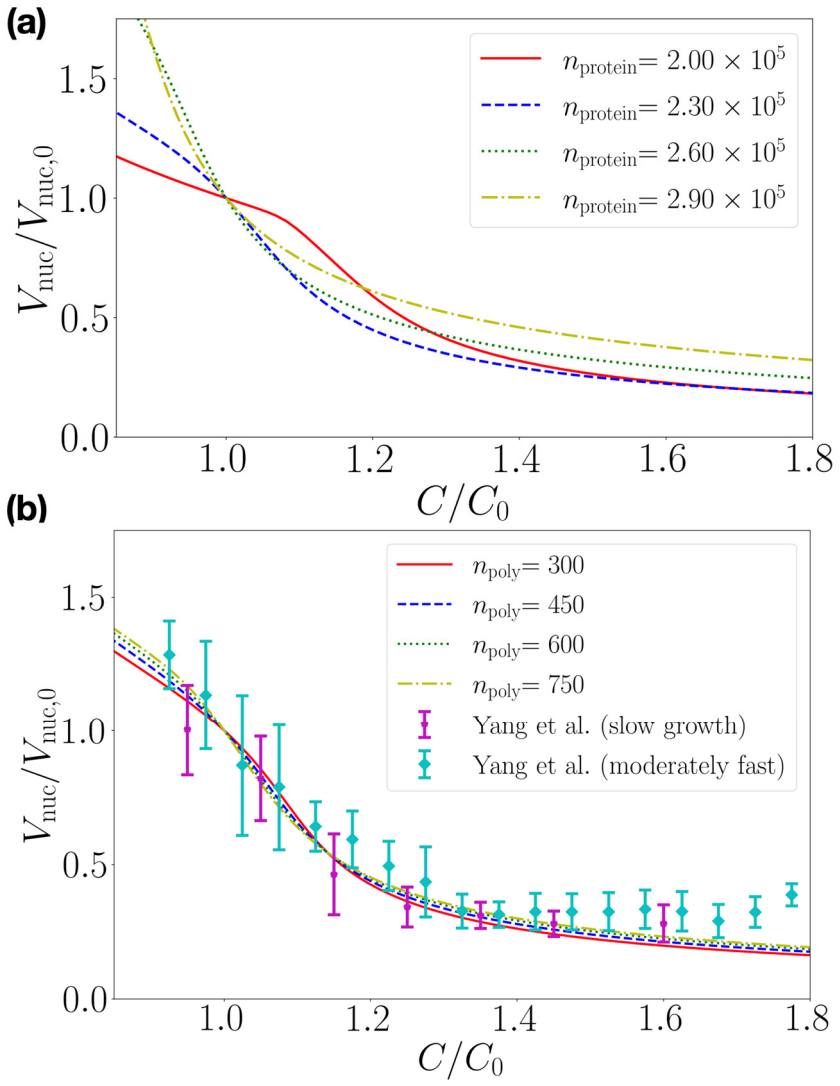

Figure 3: Scaling of the nucleoid compaction curves at different crowder numbers. In all individual curves of this figure, the number of all macromolecular crowders in the cell is fixed but the cell volume changes as in osmotic shock measurements. The volume change changes C/C_0 via relation $C/C_0 = V_{\text{cell},0}/V_{\text{cell}}$ where C_0 and $V_{\text{cell},0}$ are crowder concentration and cell volume in unperturbed cells. (a) The nucleoid compaction curves at different protein numbers. The number of polysomes is fixed for all curves ($n_{\text{poly}} = 600$). The other parameters of the model are the same as in Fig. 1c. (b) The nucleoid compaction curves for various polysome numbers. The number of proteins is fixed for all curves ($n_{\text{protein}} = 2.3 \times 10^5$). The experimental data from osmotic shock measurements from (5) at slow and moderately fast growth conditions (SI Table S3) shown by magenta and cyan points, respectively.

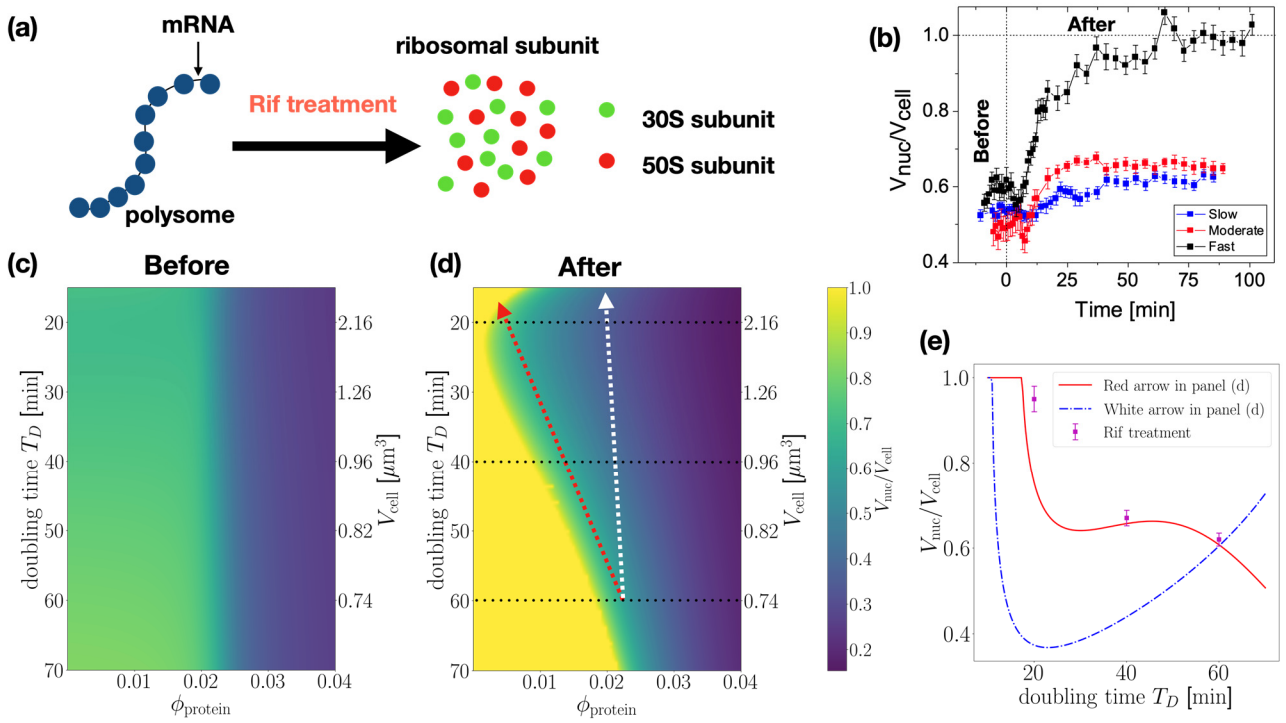

Figure 4: The growth-rate dependent expansion of the nucleoid upon dissociation of polysomes. (a) A schematic explaining the effect of the rifampicin treatment. (b) The experimentally determined change in the nucleoid to cell volume ratio as a result of treatment of *E. coli* JM57 cells with 300 µg/ml rifampicin. Treatment starts at time 0 min. The doubling times extrapolated to 37 °C are 60, 40 and 20 min corresponding to slow, moderate and fast growth rates, respectively. For the extrapolation see SI Table S3. The error bars correspond to standard error for the cell population. (c) Calculated nucleoid to cell volume ratio before the rifampicin treatment as a function of the cytosolic protein volume fraction and doubling time. The doubling times are linked to the average cell volumes (left vertical axes) via the universal bacterial growth law (SI Fig. S6a). (d) The same for rifampicin treated cells. The dashed horizontal lines show the doubling times from the experiment. The dashed white line corresponds to the change in the total protein volume fraction (including envelope layers) with the doubling time based on data in (39). The dashed red line shows a change for cytosolic volume fraction of crowding proteins that is consistent with the rifampicin treatment experiment. (e) $V_{\mathrm{nuc}}/V_{\mathrm{cell}}$ calculated along the dashed upward pointing lines of panel (d). The red line corresponds to the red dashed arrow and the blue line corresponds to the white dashed arrow. The experimental data from the plateau region of panel (b) is also shown.

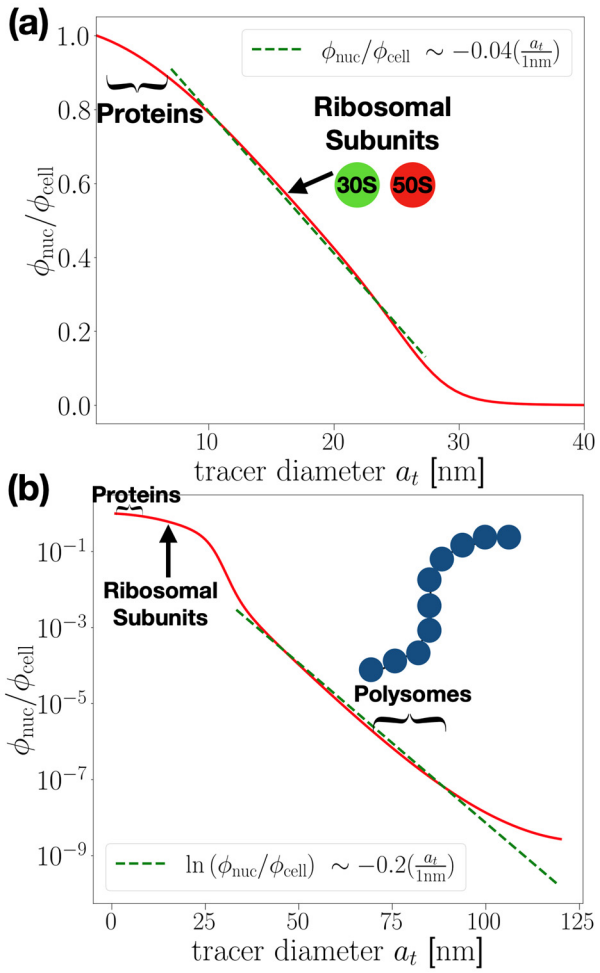

Figure 5: The dependence of the partitioning of macromolecules between the nucleoid and cytosol phases on their linear dimensions. (a) The ratio of volume fractions for the tracer particles in the nucleoid, ϕ_{nuc}, and the whole cell, ϕ_{cell}, as a function of the particle diameter a_t is displayed. A linear fit to the calculated curve from $a_t \approx 7$ nm to $a_t \approx 28$ nm is plotted with green dashed line $\phi_{nuc}/\phi_{cell} \sim -0.04\left(\frac{a_t}{1nm}\right)$. The size-ranges for proteins and ribosomal subunits in the cell are schematically shown. (b) The same curve in semi-log scale. The dashed line represents an exponentially decreasing fit to the model in the range from $a_t \approx 30$ nm to $a_t \approx 110$ nm ($\ln(\phi_{nuc}/\phi_{cell}) \sim -0.2\left(\frac{a_t}{1nm}\right)$). The size-ranges for common macromolecular crowders are schematically shown.

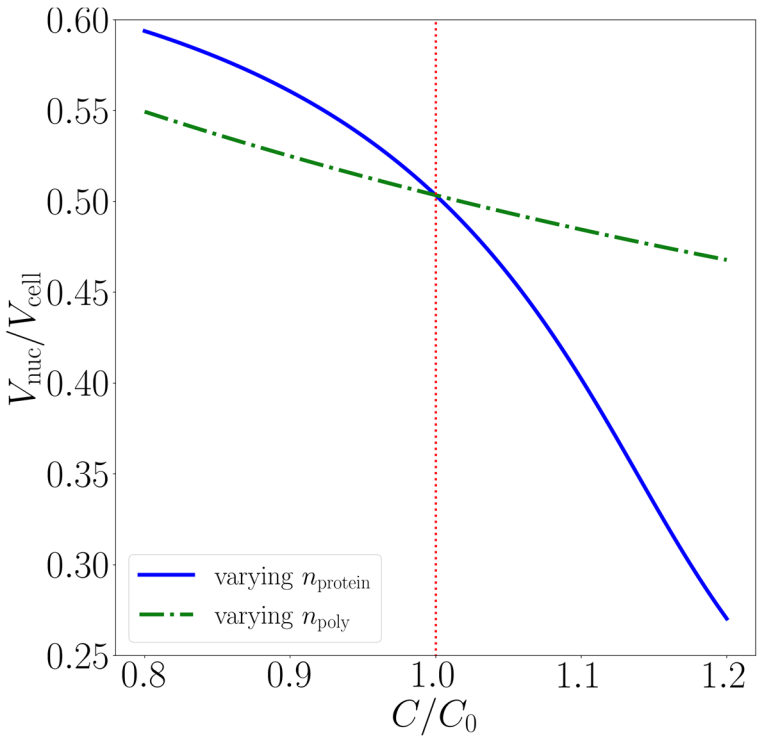

Figure 6: Differential effects arising from the fluctuations in the number of proteins and polysomes around their physiological values on the volume fraction of the nucleoid. The volume fraction of the nucleoid is displayed as a function of the normalized concentration C/C_0, where C is the number of the varying crowder species (polysomes or proteins) and C_0 is its physiological value as determined from the fitting in Fig. 1c. The cell volume V_{cell} is fixed here. The blue solid line represents the result for varying protein number while keeping the number of polysomes fixed ($n_{\mathrm{poly}} = 600$). The green dash-dotted line represents the result for varying polysome number while keeping the number of proteins fixed ($n_{\mathrm{protein}} = 2.3 \times 10^5$). The vertical, red-dotted line indicates the physiological concentration.

REFERENCES

1. Surovtsev, I.V. and C. Jacobs-Wagner. 2018. Subcellular organization: a critical feature of bacterial cell replication. Cell 172: 1271-1293.
2. Wang, X., P.M. Llopis and D.Z. Rudner. 2013. Organization and segregation of bacterial chromosomes. Nat. Rev. Genet. 14: 191-203.
3. Gogou, C., A. Japaridze and C. Dekker. 2021. Mechanisms for chromosome segregation in bacteria. Frontiers in Microbiology 12: 685687.
4. Cremer, T. and C. Cremer. 2001. Chromosome territories, nuclear architecture and gene regulation in mammalian cells. Nat. Rev. Genet. 2: 292-301.
5. Yang, D., J. Männik, S.T. Retterer and J. Männik. 2020. The effects of polydisperse crowders on the compaction of the *Escherichia coli* nucleoid. Mol Microbiol 113: 1022-1037.
6. Männik, J., D. Castillo, D. Yang, G. Siopsis and J. Männik. 2016. The role of MatP, ZapA, and ZapB in chromosomal organization and dynamics in *Escherichia coli*. Nucleic Acids Res. 44: 1216-1226.
7. Wu, F.B., P. Swain, L. Kuijpers, X. Zheng, K. Felter, M. Guurink, . . . C. Dekker. 2019. Cell boundary confinement sets the size and position of the *E. coli* chromosome. Curr. Biol. 29: 2131-2144.
8. Xiang, Y.J., I.V. Surovtsev, Y.J. Chang, S.K. Govers, B.R. Parry, J. Liu and C. Jacobs-Wagner. 2021. Interconnecting solvent quality, transcription, and chromosome folding in *Escherichia coli*. Cell 184: 3626-3642.
9. Gray, W.T., S.K. Govers, Y.J. Xiang, B.R. Parry, M. Campos, S. Kim and C. Jacobs-Wagner. 2019. Nucleoid size scaling and intracellular organization of translation across bacteria. Cell 177: 1632-1648.
10. Cunha, S., C.L. Woldringh and T. Odijk. 2001. Polymer-mediated compaction and internal dynamics of isolated *Escherichia coli* nucleoids. J. Struct. Biol. 136: 53-66.
11. Romantsov, T., I. Fishov and O. Krichevsky. 2007. Internal structure and dynamics of isolated *Escherichia coli* nucleoids assessed by fluorescence correlation spectroscopy. Biophys. J. 92: 2875-2884.
12. de Vries, R. 2010. DNA condensation in bacteria: interplay between macromolecular crowding and nucleoid proteins. Biochimie 92: 1715-1721.
13. Jin, D.J., C. Cagliero and Y.N. Zhou. 2013. Role of RNA polymerase and transcription in the organization of the bacterial nucleoid. Chemical Reviews 113: 8662-8682.
14. Dame, R.T., F.Z.M. Rashid and D.C. Grainger. 2020. Chromosome organization in bacteria: mechanistic insights into genome structure and function. Nat. Rev. Genet. 21: 227-242.
15. Makela, J., S. Uphoff and D.J. Sherratt. 2021. Nonrandom segregation of sister chromosomes by *Escherichia coli* MukBEF. Proc. Natl. Acad. Sci. U. S. A. 118: e2022078118.
16. Lioy, V.S., A. Cournac, M. Marbouty, S. Duigou, J. Mozziconacci, O. Espeli, . . . R. Koszul. 2018. Multiscale structuring of the *E. coli* chromosome by nucleoid-associated and condensin proteins. Cell 172: 771-783.
17. Cristofalo, M., C.A. Marrano, D. Salerno, R. Corti, V. Cassina, A. Mammola, . . . F. Mantegazza. 2020. Cooperative effects on the compaction of DNA fragments by the nucleoid protein H-NS and the crowding agent PEG probed by Magnetic Tweezers. Biochimica et Biophysica Acta (BBA) - General Subjects 1864: 129725.
18. Meyer, A.S. and D.C. Grainger. (2013) In Sariaslani, S. and Gadd, G. M. (eds.), *Advances in Applied Microbiology*. Academic Press, Vol. 83, pp. 69-86.
19. Woldringh, C.L., P.R. Jensen and H.V. Westerhoff. 1995. Structure and partitioning of bacterial DNA: determined by a balance of compaction and expansion forces. FEMS Microbiol. Lett. 131: 235-242.
20. Zimmerman, S.B. and L.D. Murphy. 1996. Macromolecular crowding and the mandatory condensation of DNA

in bacteria. Febs Letters 390: 245-248.

21. Männik, J., T.F. Teshima, B. Wolfrum and D. Yang. 2021. Lab-on-a-chip based mechanical actuators and sensors for single-cell and organoid culture studies. J Appl Phys 129: 210905.

22. Pelletier, J., K. Halvorsen, B.-Y. Ha, R. Paparcone, S.J. Sandler, C.L. Woldringh, . . . S. Jun. 2012. Physical manipulation of the *Escherichia coli* chromosome reveals its soft nature. Proc. Natl. Acad. Sci. U. S. A. 109: E2649-E2656.

23. Odijk, T. 1998. Osmotic compaction of supercoiled DNA into a bacterial nucleoid. Biophys. Chem. 73: 23-29.

24. Jeon, C., Y. Jung and B.Y. Ha. 2016. Effects of molecular crowding and confinement on the spatial organization of a biopolymer. Soft Matter 12: 9436-9450.

25. Joyeux, M. 2018. A segregative phase separation scenario of the formation of the bacterial nucleoid. Soft Matter 14: 7368-7381.

26. Joyeux, M. 2020. Bacterial nucleoid: interplay of DNA demixing and supercoiling. Biophys. J. 118: 2141-2150.

27. Shendruk, T.N., M. Bertrand, H.W. de Haan, J.L. Harden and G.W. Slater. 2015. Simulating the Entropic Collapse of Coarse-Grained Chromosomes. Biophys. J. 108: 810-820.

28. Shin, J., A.G. Cherstvy and R. Metzler. 2014. Mixing and segregation of ring polymers: spatial confinement and molecular crowding effects. New Journal of Physics 16: 053047.

29. Ehrenberg, M., H. Bremer and P.P. Dennis. 2013. Medium-dependent control of the bacterial growth rate. Biochimie 95: 643-658.

30. Dai, X.F., M.L. Zhu, M. Warren, R. Balakrishnan, V. Patsalo, H. Okano, . . . T. Hwa. 2017. Reduction of translating ribosomes enables *Escherichia coli* to maintain elongation rates during slow growth. Nature Microbiology 2: 16231.

31. Mondal, J., B.P. Bratton, Y.J. Li, A. Yethiraj and J.C. Weisshaar. 2011. Entropy-based mechanism of ribosome-nucleoid segregation in *E. coli* cells. Biophys. J. 100: 2605-2613.

32. Joyeux, M. 2016. *In vivo* compaction dynamics of bacterial DNA: a fingerprint of DNA/RNA demixing? Current Opinion in Colloid & Interface Science 26: 17-27.

33. Joyeux, M. 2017. Coarse-grained model of the demixing of DNA and non-binding globular macromolecules. Journal of Physical Chemistry B 121: 6351-6358.

34. Miangolarra, A.M., S.H.J. Li, J.F. Joanny, N.S. Wingreen and M. Castellana. 2021. Steric interactions and out-of-equilibrium processes control the internal organization of bacteria. Proc. Natl. Acad. Sci. U. S. A. 118: e2106014118.

35. Kim, J., C. Jeon, H. Jeong, Y. Jung and B.Y. Ha. 2015. A polymer in a crowded and confined space: effects of crowder size and poly-dispersity. Soft Matter 11: 1877-1888.

36. Kellenberger, E., A. Ryter and J. Sechaud. 1958. Electron microscope study of DNA-containing plasms. 2. Vegetative and mature phage DNA as compared with normal bacterial nucleoids in different physiological states. J Biophys Biochem Cy 4: 671.

37. Bakshi, S., H. Choi and J.C. Weisshaar. 2015. The spatial biology of transcription and translation in rapidly growing *Escherichia coli*. Frontiers in Microbiology,doi: 10.3389/fmicb.2015.00636.

38. Bakshi, S., A. Siryaporn, M. Goulian and J.C. Weisshaar. 2012. Superresolution imaging of ribosomes and RNA polymerase in live *Escherichia coli* cells. Mol. Microbiol. 85: 21-38.

39. Balakrishnan, R., M. Mori, I. Segota, Z.G. Zhang, R. Aebersold, C. Ludwig and T. Hwa. 2022. Principles of gene regulation quantitatively connect DNA to RNA and proteins in bacteria. Science 378: 1066.

40. Boles, T.C., J.H. White and N.R. Cozzarelli. 1990. Structure of plectonemically supercoiled DNA. Journal of

Molecular Biology 213: 931-951.

41. Rubinstein, M. and R. Colby. (2003) *Polymer Physics*. Oxford University Press, New York.

42. Chen, H., S.P. Meisburger, S.A. Pabit, J.L. Sutton, W.W. Webb and L. Pollack. 2012. Ionic strength-dependent persistence lengths of single-stranded RNA and DNA. Proc. Natl. Acad. Sci. U. S. A. 109: 799-804.

43. Fleer, G.J., A.M. Skvortsov and R. Tuinier. 2007. A simple relation for the concentration dependence of osmotic pressure and depletion thickness in polymer solutions. Macromol Theor Simul 16: 531-540.

44. Schäfer, L. (1999) *Excluded volume effects in polymer solutions, as explained by the renormalization group*. Springer, Berlin.

45. Gao, F. and L. Han. 2012. Implementing the Nelder-Mead simplex algorithm with adaptive parameters. Computational Optimization and Applications 51: 259-277.

46. Wegner, A.S., S. Alexeeva, T. Odijk and C.L. Woldringh. 2012. Characterization of *Escherichia coli* nucleoids released by osmotic shock. J. Struct. Biol. 178: 260-269.

47. Milo, R. 2013. What is the total number of protein molecules per cell volume? A call to rethink some published values. Bioessays 35: 1050-1055.

48. Koch, A.L. 1983. The surface stress theory of microbial morphogenesis. Adv Microb Physiol 24: 301-366.

49. Dworsky, P. and M. Schaechter. 1973. Effect of rifampin on the structure and membrane attachment of the nucleoid of Escherichia coli. J Bacteriol 116: 1364-1374.

50. Bakshi, S., H. Choi, J. Mondal and J.C. Weisshaar. 2014. Time-dependent effects of transcription- and translation-halting drugs on the spatial distributions of the *Escherichia coli* chromosome and ribosomes. Mol. Microbiol. 94: 871-887.

51. Sanamrad, A., F. Persson, E.G. Lundius, D. Fange, A.H. Gynna and J. Elf. 2014. Single-particle tracking reveals that free ribosomal subunits are not excluded from the *Escherichia coli* nucleoid. Proc. Natl. Acad. Sci. U. S. A. 111: 11413-11418.

52. Pettijohn, D.E. and R. Hecht. 1974. RNA molecules bound to the folded bacterial genome stabilize DNA folds and segregate domains of supercoiling. Cold Spring Harb Symp Quant Biol 38: 31-41.

53. Bremer, H. and P.P. Dennis. 2008. Modulation of Chemical Composition and Other Parameters of the Cell at Different Exponential Growth Rates. EcoSal Plus 3.

54. van den Berg, J., A.J. Boersma and B. Poolman. 2017. Microorganisms maintain crowding homeostasis. Nat. Rev. Microbiol. 15: 309-318.

55. Irastortza-Olaziregi, M. and O. Amster-Choder. 2021. Coupled transcription-translation in prokaryotes: an old couple with new surprises. Frontiers in Microbiology,doi: 624830 10.3389/fmicb.2020.624830.

56. Kohram, M. (2021) Ph. D. Dissertation, University of Pittsburgh.

Supporting Information for

Differentiating the roles of proteins and polysomes in nucleoid size homeostasis in *Escherichia coli*

Mu-Hung Chang[1], Maxim O. Lavrentovich*[1,2,] and Jaan Männik*[1]

[1]Department of Physics and Astronomy, The University of Tennessee, Knoxville, TN 37996, USA
[2]Department of Earth, Environment, and Physics, Worcester State University, Worcester, MA 01602, USA

This PDF file includes:

Supporting Information Text
Figures S1 to S7
Tables S1 to S3
References for SI reference citations

Correspondence: mlavrent@utk.edu, jmannik@utk.edu

SI Text

SI Text provides a more detailed description for individual terms in the free energy model, notes on minimizing the free energy numerically and formulas expressing growth rate dependence of the *E. coli* cytosolic components.

Free energy terms describing the corresponding crowder-only system, F_0

In the Eq. 1 of the main text, we use F_0 to denote several free energy terms describing the corresponding crowder-only system. Here we discuss these terms in detail.

1) Translational free energy. For a mixture of a polymer and solvent, the ideal free energy of mixing (derived via a Flory-Huggins model, say (1)) is given by

$$F = n \ln \phi - Nn, \tag{S1}$$

where n is the number of polymers and N is the degree of polymerization (monomers per polymer). We use $N = N_{\mathrm{ribo}} = 10$ for polysomes and $N = 1$ for proteins. The ideal entropic free energy of polysomes and proteins can then be written as

$$F_{\mathrm{ideal}} = n_{\mathrm{poly}} \ln \phi_{\mathrm{poly}} - N_{\mathrm{ribo}} n_{\mathrm{poly}} + n_{\mathrm{protein}} \ln \phi_{\mathrm{protein}} - n_{\mathrm{protein}}. \tag{S2}$$

2) Internal free energy of polysomes. We represent polysomes as a "beads-on-a-string" polymer. The beads are ribosomes of diameter $a_{\mathrm{ribo}} = 20$ nm, and the string is mRNA. Since mRNA is highly flexible, we estimate the Kuhn length for this polymer as $b = a_{\mathrm{ribo}}$. To account for the free energy associated with the entropy and excluded volume interactions in a single polysome, we use the Flory formula (1):

$$F_{\mathrm{Flory}} \sim \frac{a_{\mathrm{ribo}}^3 N_{\mathrm{ribo}}^2}{\left(R_{\mathrm{g}}^{\mathrm{poly}}\right)^3} + \frac{\left(R_{\mathrm{g}}^{\mathrm{poly}}\right)^2}{\mathrm{N_{ribo}} a_{\mathrm{ribo}}^2}. \tag{S3}$$

where R_g^{poly} is the radius of gyration of the polysome. Here, the first term represents the excluded volume interactions while the second term is an entropic contribution from the various possible polymer configurations. We minimize the total free energy of the system with respect to the radius of gyration R_g^{poly}, which may be different in the nucleoid and cytosol phases due to the crowding conditions. We find that R_g^{poly} varies relatively little from normal cells to strongly osmotically shocked cells, with a typical value $R_g^{\mathrm{poly}} \approx 35$ nm. Note that this value is quite a bit smaller than the estimate for a free polysome in

solution, in which case $R = \left(\frac{3N^3}{2}\right)^{1/5} a_{\text{ribo}} \approx 90$ nm. This indicates that the DNA-polysome and protein-polysome interactions play an important role in compacting the polysome. We consider these terms in the following sections.

3) Protein-protein interaction free energy. We model proteins as hard spheres with diameter $a_p = 5$ nm. For such a collection of hard spheres, the equation of state can be well approximated by the Carnahan-Starling form (2)

$$\frac{\Pi V}{n} = \frac{1 + \phi + \phi^2 - \phi^3}{(1-\phi)^3}, \tag{S4}$$

where V is the total available volume, Π is the osmotic pressure, n is the number of particles, and $\phi = \frac{n v_0}{V}$ is the volume fraction. To find the free energy we integrate up the osmotic pressure as follows:

$$F = \int \left[\frac{\partial F}{\partial V}\right]_{n,T} dV = -\int \Pi dV = n \int \frac{1 + \phi + \phi^2 - \phi^3}{\phi(1-\phi)^3} d\phi = n\left[\ln \phi + \frac{3 - 2\phi}{(1-\phi)^2} + \text{constant}\right]. \tag{S5}$$

This free energy is a sum of entropic and interaction terms. Eq. S5 should reduce to the ideal entropic term (Eq. S1) when $\phi \to 0$. It follows, then, that the integration constant must be equal to -4 and the non-ideal term can be written as

$$F_{\text{CS}} = n \frac{4\phi - 3\phi^2}{(1-\phi)^2}. \tag{S6}$$

F_{CS} describes the non-ideal free energy contribution due to the protein-protein interaction. Taken together, the free energy F_0 (Eq. 1 of the main text) corresponding to protein-protein interactions reads

$$F_0 = F_{\text{ideal}} + F_{\text{Flory}} + F_{\text{CS}}. \tag{S7}$$

DNA self-interaction

This section extends the discussion of the free energy for an isolated compressed DNA in the main text. This contribution reads

$$F_{\text{DNA}} = g\left(\frac{V_{\text{nuc,free}}}{V_{\text{nuc}}}\right)^{\alpha}, \tag{S8}$$

where V_{nuc} is the volume of the DNA in confined conditions and $V_{\text{nuc,free}}$ is the volume of a liberated DNA in solution. In this semi-empirical expression, the value of α is linked to ν, the Flory exponent. The Flory exponent can be calculated using the "blob model". To simplify the discussion, let's assume that $g = 1$. Consider the DNA consisting of N_{blob} blobs corresponding to a local region of DNA which can be treated

as an ideal chain. Each blob has a diameter of ξ and contains m DNA monomers. In confined conditions, the blob diameter ξ decreases compared to the value ξ_0 in solution (where the entire DNA consists of a single blob). Under confined conditions, each blob contributes a free energy k_BT, so we may write $F_{\mathrm{DNA}} = N_{\mathrm{blob}}$ in units of k_BT. The Flory exponent tells us how the blob size scales with the number of DNA monomers m: $\xi \sim m^{\nu} b_{\mathrm{DNA}}$, where b_{DNA} is the size of a DNA monomer. The volume of each blob is $V_{\mathrm{blob}} \sim \xi^3$. For free (unconfined) DNA, the volume is instead given by $V_{\mathrm{nuc,free}} \sim \xi_0^3$, where ξ_0 is estimated as $\xi_0 \sim b_{\mathrm{DNA}} N_{\mathrm{DNA}}^{\nu}$. Given that $N_{\mathrm{DNA}} = mN_{\mathrm{blob}}$ is the total number of monomers in DNA in the confined conditions, it follows that we can write the total number of blobs as

$$N_{\mathrm{blob}} = \frac{N_{\mathrm{DNA}}}{m} = \left(\frac{\xi_0}{\xi}\right)^{1/\nu}, \tag{S9}$$

from which it is clear that $N_{\mathrm{blob}} = 1$ when $\xi = \xi_0$. On the other hand, from Eq. S8, we have that the free energy should be

$$F_{\mathrm{DNA}} = N_{\mathrm{blob}} = \left(\frac{V_{\mathrm{nuc,free}}}{V_{\mathrm{nuc}}}\right)^{\alpha} = \left(\frac{\xi_0^3}{N_{\mathrm{blob}}\xi^3}\right)^{\alpha} = (N_{\mathrm{blob}})^{\alpha(3\nu-1)}, \tag{S10}$$

which means that the fractal dimension must be related to the exponent α via

$$\nu = (1+\alpha)/3\alpha. \tag{S11}$$

We find $\alpha \approx 0.85$ from the fit of the model to the experimental data and the corresponding Flory exponent $\nu \approx 0.73$. The Flory exponent is also sometimes equated to the inverse mass fractal dimension. The corresponding fractal dimension of DNA is therefore $D_f \approx 1.37$. This low fractal dimension is consistent with *in vivo* experiments where the chromosome was found to form a linearly-ordered nucleoid filament (3), implying $D_f \approx 1$. However, theoretical analysis of the diffusion of chromosomal loci (4) and recent experimental work (5) have come to conclude a much higher fractal dimension close to 3 (the experimental work found $D_f = 2.78$ (5)). The discrepancy might be related to different spatial scales involved in diffusion experiments (small spatial scale) and in the experiments here (large spatial scale encompassing the whole chromosome). It is also possible that the arguments we brought forward for the blob-model above are not valid for the bacterial nucleoid. In that case, the exponent α should just be considered as an empirical parameter describing the non-linear compressibility of the nucleoid (see additional discussion below).

To understand how the variations in $\boldsymbol{\alpha}$ and $\boldsymbol{g}$ affect the outcomes of the model, we plot compaction curves

for various $\boldsymbol{g}$ and $\boldsymbol{\alpha}$ values about their best fit values ($\boldsymbol{\alpha = 0.85}$ and $\boldsymbol{g = 145}$). The increase in both $\boldsymbol{\alpha}$ and $\boldsymbol{g}$ leads to larger nucleoids (Fig. S1b,c). The effect is more pronounced for the exponent $\boldsymbol{\alpha}$. Also, note that the increase in $\boldsymbol{g}$ is equivalent to increase in $\boldsymbol{V_{\mathrm{nuc,free}}}$. Increased $\boldsymbol{V_{\mathrm{nuc,free}}}$ leads, expectedly, also to larger $\boldsymbol{V_{\mathrm{nuc}}}$. Increase in $\boldsymbol{\alpha}$ decreases the compressibility, $\boldsymbol{\beta}_{\mathrm{DNA}}$, of the nucleoid (the inverse of the bulk modulus $\boldsymbol{\beta}_{\mathrm{DNA}} = \boldsymbol{1/\kappa}_{\mathrm{DNA}}$) since $\boldsymbol{\kappa}_{\mathrm{DNA}}$ is given as

$$\boldsymbol{\kappa}_{\mathrm{DNA}} \equiv \boldsymbol{V}_{\mathrm{nuc}} \frac{\boldsymbol{\partial^2 F}_{\mathrm{DNA}}}{\boldsymbol{\partial V}_{\mathrm{nuc}}^2} = \frac{\boldsymbol{g\alpha(\alpha+1)}}{\boldsymbol{V}_{\mathrm{nuc}}} \left(\frac{\boldsymbol{V}_{\mathrm{nuc,free}}}{\boldsymbol{V}_{\mathrm{nuc}}}\right)^{\boldsymbol{\alpha}}. \qquad \mathbf{(S12)}$$

The equation indicates that the nucleoid is more "compactable" when $\boldsymbol{\alpha}$ is small.

Polysome-polysome interaction

To calculate the polysome-polysome interaction free energy, we use a result from the theory of polymer solutions (1). The osmotic pressure (as explained in the main text) is well-approximated by

$$\Pi = \frac{n_{\mathrm{poly}}}{V}\left[1 + \left(\frac{\phi_{\mathrm{poly}}}{0.69\phi_{\mathrm{ov}}}\right)^{1.309}\right], \qquad (5), (\mathrm{S13})$$

where $\boldsymbol{n}_{\mathrm{poly}}$ is the number of polysomes and $\boldsymbol{\phi}_{\mathrm{poly}}$ is their volume fraction. The overlap volume fraction $\boldsymbol{\phi}_{\mathrm{ov}}$ is defined as $\boldsymbol{\phi}_{\mathrm{ov}} \equiv \frac{\boldsymbol{Nb^3}}{\boldsymbol{R_g^3}}$, where $\boldsymbol{b}$ is the size of a single monomer and $\boldsymbol{R_g}$ is the radius of gyration of the polysome. The expression of osmotic pressure combines the limiting behaviors in dilute and semidilute regimes (6), and the exponent 1.309 follows the result from the renormalization group calculation (7). To find the interaction free energy we integrate as follows:

$$\boldsymbol{F} = -\int \boldsymbol{\Pi dV} = \int \frac{\boldsymbol{n}}{\boldsymbol{\phi}}\left[\mathbf{1} + \left(\frac{\boldsymbol{\phi}}{\mathbf{0.69}\boldsymbol{\phi}_{\mathrm{ov}}}\right)^{\mathbf{1.309}}\right] \boldsymbol{d\phi} = \boldsymbol{n\, ln\, \phi} + \frac{\boldsymbol{n}}{\mathbf{1.309}}\left(\frac{\boldsymbol{\phi}}{\mathbf{0.69}\boldsymbol{\phi}_{\mathrm{ov}}}\right)^{\mathbf{1.309}} + \mathrm{const.} \quad \boldsymbol{(S14)}$$

This free energy contribution should reduce to the entropic free energy term (Eq. S1) when $\boldsymbol{\phi \to 0}$, which tells us the integration constant is $\boldsymbol{-nN}$. Therefore, the non-ideal polysome-polysome interaction can be identified as $\boldsymbol{F}_{\text{poly-poly}} = \frac{\boldsymbol{n}_{\mathrm{poly}}}{\mathbf{1.309}}\left(\frac{\boldsymbol{\phi}}{\mathbf{0.69}\boldsymbol{\phi}_{\mathrm{ov}}}\right)^{\mathbf{1.309}}$, as given by Eq. 6 in the main text.

Interaction between polysomes and other spherical species (proteins and tracer particle)

Since we treat polysomes as a "beads-on-a-string" polymer, the interaction between polysomes and other spherical species must differ from the simple pairwise interaction between hard spheres. We consider the polysome excluded volume interaction between polysomes and other hard spherical particles as

$$F = n_{\text{poly}} n_{\text{sp}} \frac{B_{\text{poly-sp}}}{V}, \tag{S15}$$

where $B_{\text{poly–sp}}$ is the first-order virial coefficient describing the excluded volume of a polysome and a spherical particle. If the size of crowder particle is small compared to the radius of gyration of polysomes R_g^{poly}, the spherical crowder will interact with individual ribosomes. Otherwise, the spherical crowders experience excluded volume interactions from the polymeric polysomes. In this case, we may use an equivalent hard sphere model for the polysome, with an effective radius $r_{\text{poly}}^{\text{eff}} = \sqrt{\frac{5}{3}} R_g^{\text{poly}}$ (8). We may then write the virial coefficient $B_{\text{poly–sp}}$ as

$$B_{\text{poly-sp}} = f\left[\frac{4\pi}{3}\left(r_{\text{poly}}^{\text{eff}} + r_{\text{sp}}\right)^3\right] + (1-f)\left[\frac{4\pi}{3} N_{\text{ribo}}\left(r_{\text{ribo}} + r_{\text{sp}}\right)^3\right], \tag{S16}$$

where $N_{\text{ribo}} = 10$ and r_{sp} is the radius of the spherical crowder particle. As in the DNA-crowder interaction, we introduce an empirical function f characterizing the transition between the two excluded volume regimes for small ($r_{\text{sp}} \ll R_g^{\text{poly}}$) and large ($r_{\text{sp}} \gg R_g^{\text{poly}}$) crowder particles. The function is given by

$$f \equiv \frac{1}{2}\left[1 + \tanh\left(\frac{r_{\text{sp}} - R_g^{\text{poly}}}{\xi_{\text{poly}}}\right)\right], \tag{S17}$$

where ξ_{poly} is the characteristic length used to regulate the width of the transition zone between the two regimes. In this study, the value of ξ_{poly} is set to 10 nm. The $F_{\text{poly-protein}}$ in Eq. 1 of the main text is then given as

$$F_{\text{poly-protein}} = n_{\text{poly}} n_{\text{protein}} \frac{B_{\text{poly-protein}}}{V}. \tag{S18}$$

Total free energy of the system

In this section, we write Eq. 1 in the main text as a more explicit expression, combining each term described above and in the main text. For the nucleoid phase, the total free energy is given as

$$F_{\text{nuc}} = \underbrace{n_{\text{nuc}}^{\text{poly}} \ln \phi_{\text{nuc}}^{\text{poly}} - N_{\text{ribo}} n_{\text{nuc}}^{\text{poly}} + n_{\text{nuc}}^{\text{protein}} \ln \phi_{\text{nuc}}^{\text{protein}} - n_{\text{nuc}}^{\text{protein}}}_{\text{entropic}} + \underbrace{n_{\text{nuc}}^{\text{protein}} \frac{4\phi_{\text{nuc}}^{\text{protein}} - 3\left(\phi_{\text{nuc}}^{\text{protein}}\right)^2}{\left(1 - \phi_{\text{nuc}}^{\text{protein}}\right)^2}}_{\text{Carnahan-Starling}}$$

$$+ \underbrace{n_{\text{nuc}}^{\text{poly}} \left[\frac{a_{\text{ribo}}^3 N_{\text{ribo}}^2}{\left(R_g^{\text{poly,nuc}}\right)^3} + \frac{\left(R_g^{\text{poly,nuc}}\right)^2}{N_{\text{ribo}} a_{\text{ribo}}^2}\right]}_{\text{Flory}} + \underbrace{g\left(\frac{V_{\text{DNA,free}}}{V_{\text{nuc}}}\right)^{\alpha}}_{\text{DNA}} + \underbrace{n_{\text{nuc}}^{\text{poly}} \frac{B_{\text{DNA-poly}}}{V_{\text{nuc}}}}_{\text{DNA-polysome}} + \underbrace{n_{\text{nuc}}^{\text{protein}} \frac{B_{\text{DNA-protein}}}{V_{\text{nuc}}}}_{\text{DNA-protein}}$$

$$+\underbrace{n_{\mathrm{nuc}}^{\mathrm{poly}} n_{\mathrm{nuc}}^{\mathrm{protein}} \frac{B_{\mathrm{nuc}}^{\text{poly-protein}}}{V_{\mathrm{nuc}}}}_{\text{polysome-protein}} + \underbrace{\frac{n_{\mathrm{nuc}}^{\mathrm{poly}}}{1.309}\left(\frac{\phi_{\mathrm{nuc}}^{\mathrm{poly}}}{0.69\phi_{\mathrm{nuc,ov}}}\right)^{1.309}}_{\text{polysome-polysome}},$$

(S19)

and for the cytosol phase

$$F_{\mathrm{cyto}} = \underbrace{n_{\mathrm{cyto}}^{\mathrm{poly}} \ln \phi_{\mathrm{cyto}}^{\mathrm{poly}} - N_{\mathrm{ribo}} n_{\mathrm{cyto}}^{\mathrm{poly}} + n_{\mathrm{cyto}}^{\mathrm{protein}} \ln \phi_{\mathrm{cyto}}^{\mathrm{protein}} - n_{\mathrm{cyto}}^{\mathrm{protein}}}_{\text{entropic}} + \underbrace{n_{\mathrm{cyto}}^{\mathrm{protein}} \frac{4\phi_{\mathrm{cyto}}^{\mathrm{protein}} - 3\left(\phi_{\mathrm{cyto}}^{\mathrm{protein}}\right)^2}{\left(1-\phi_{\mathrm{cyto}}^{\mathrm{protein}}\right)^2}}_{\text{Carnahan-Starling}}$$

$$+\underbrace{n_{\mathrm{cyto}}^{\mathrm{poly}}\left[\frac{a_{\mathrm{ribo}}^3 N_{\mathrm{ribo}}^2}{\left(R_g^{\mathrm{poly,cyto}}\right)^3} + \frac{\left(R_g^{\mathrm{poly,cyto}}\right)^2}{N_{\mathrm{ribo}} a_{\mathrm{ribo}}^2}\right]}_{\text{Flory}} + \underbrace{n_{\mathrm{cyto}}^{\mathrm{poly}} n_{\mathrm{cyto}}^{\mathrm{protein}} \frac{B_{\mathrm{cyto}}^{\text{poly-protein}}}{V_{\mathrm{cyto}}}}_{\text{polysome-protein}} + \underbrace{\frac{n_{\mathrm{cyto}}^{\mathrm{poly}}}{1.309}\left(\frac{\phi_{\mathrm{cyto}}^{\mathrm{poly}}}{0.69\phi_{\mathrm{cyto,ov}}}\right)^{1.309}}_{\text{polysome-polysome}},$$

(S20)

where $n_{\mathrm{cyto}} \equiv n_{\mathrm{cell}} - n_{\mathrm{nuc}}$ and $V_{\mathrm{cyto}} \equiv V_{\mathrm{cell}} - V_{\mathrm{nuc}}$. The total free energy of the system with the two distinct nucleoid and cytosol phases is then written as $F_{\mathrm{demix}} = F_{\mathrm{nuc}} + F_{\mathrm{cyto}}$. The free energy of the system with a single mixed phase (no nucleoid formed) is given in a similar fashion as

$$F_{\mathrm{mix}} = \underbrace{n_{\mathrm{cell}}^{\mathrm{poly}} \ln \phi_{\mathrm{cell}}^{\mathrm{poly}} - N_{\mathrm{ribo}} n_{\mathrm{cell}}^{\mathrm{poly}} + n_{\mathrm{cell}}^{\mathrm{protein}} \ln \phi_{\mathrm{cell}}^{\mathrm{protein}} - n_{\mathrm{cell}}^{\mathrm{protein}}}_{\text{entropic}} + \underbrace{n_{\mathrm{cell}}^{\mathrm{protein}} \frac{4\phi_{\mathrm{cell}}^{\mathrm{protein}} - 3\left(\phi_{\mathrm{cell}}^{\mathrm{protein}}\right)^2}{\left(1-\phi_{\mathrm{cell}}^{\mathrm{protein}}\right)^2}}_{\text{Carnahan-Starling}}$$

$$+\underbrace{n_{\mathrm{cell}}^{\mathrm{poly}}\left[\frac{a_{\mathrm{ribo}}^3 N_{\mathrm{ribo}}^2}{\left(R_g^{\mathrm{poly,mix}}\right)^3} + \frac{\left(R_g^{\mathrm{poly,mix}}\right)^2}{N_{\mathrm{ribo}} a_{\mathrm{ribo}}^2}\right]}_{\text{Flory}} + \underbrace{g\left(\frac{V_{\mathrm{DNA,free}}}{V_{\mathrm{cell}}}\right)^{\alpha}}_{\text{DNA}} + \underbrace{n_{\mathrm{cell}}^{\mathrm{poly}} \frac{B_{\text{DNA-poly}}}{V_{\mathrm{cell}}}}_{\text{DNA-polysome}} + \underbrace{n_{\mathrm{cell}}^{\mathrm{protein}} \frac{B_{\text{DNA-protein}}}{V_{\mathrm{cell}}}}_{\text{DNA-protein}}$$

$$+\underbrace{n_{\mathrm{cell}}^{\mathrm{poly}} n_{\mathrm{cell}}^{\mathrm{protein}} \frac{B_{\mathrm{cell}}^{\text{poly-protein}}}{V_{\mathrm{cell}}}}_{\text{polysome-protein}} + \underbrace{\frac{n_{\mathrm{cell}}^{\mathrm{poly}}}{1.309}\left(\frac{\phi_{\mathrm{cell}}^{\mathrm{poly}}}{0.69\phi_{\mathrm{cell,ov}}}\right)^{1.309}}_{\text{polysome-polysome}}$$

(S21)

where the subscript "cell" indicates the corresponding quantity in the whole cell. Notice that, in order to evaluate F_{mix}, it is necessary to first determine $R_g^{\mathrm{poly,mix}}$, which represents the radius of gyration of polysomes in the mixed phase. We thus first minimize Eq. S21 with respect to $R_g^{\mathrm{poly,mix}}$ to determine its value at the minimum F_{mix}. Next, to study the formation and properties of the nucleoid, we minimize the free energy difference between the demixed and mixed states, $\Delta F = F_{\mathrm{demix}} - F_{\mathrm{mix}}$, with respect to the

nucleoid phase volume V_{nuc} in the demixed state, the numbers of each crowder species in the nucleoid phase ($n_{\mathrm{nuc}}^{\mathrm{protein}}$, $\mathrm{n}_{\mathrm{nuc}}^{\mathrm{poly}}$), and the radii of gyration of polysomes in the nucleoid and cytosol phases ($R_g^{\mathrm{poly,nuc}}$, $R_g^{\mathrm{poly,cyto}}$). The formation of a nucleoid occurs if $\Delta F < 0$ at the minimum.

Osmotic pressure from crowders

We can estimate the balance of osmotic pressures at the boundary between the nucleoid and cytosol phases by combining Eq. S19 and S20 with the following expression for the osmotic pressure: $\Pi = -\left(\frac{\partial F}{\partial V}\right)_{T,n}$. Taking the derivative of Eq. S19 with respect to V_{nuc} gives

$$\Pi_{\mathrm{nuc}} = \underbrace{\frac{n_{\mathrm{nuc}}^{\mathrm{protein}}\left[1+\phi_{\mathrm{nuc}}^{\mathrm{protein}}+\left(\phi_{\mathrm{nuc}}^{\mathrm{protein}}\right)^2-\left(\phi_{\mathrm{nuc}}^{\mathrm{protein}}\right)^3\right]}{V_{\mathrm{nuc}}\left(1-\phi_{\mathrm{nuc}}^{\mathrm{protein}}\right)^3}}_{\text{protein}} + \underbrace{\frac{n_{\mathrm{nuc}}^{\mathrm{poly}}}{V_{\mathrm{nuc}}}\left[1+\left(\frac{\phi_{\mathrm{nuc}}^{\mathrm{poly}}}{0.69\phi_{\mathrm{nuc,ov}}}\right)^{1.309}\right]}_{\text{polysome}}$$
$$+ \underbrace{\frac{g\alpha}{V_{\mathrm{nuc}}}\left(\frac{V_{\mathrm{DNA,free}}}{V_{\mathrm{nuc}}}\right)^{\alpha}}_{\text{DNA}} + \underbrace{n_{\mathrm{nuc}}^{\mathrm{poly}}\frac{B_{\text{DNA-poly}}}{V_{\mathrm{nuc}}^2}}_{\text{DNA-polysome}} + \underbrace{n_{\mathrm{nuc}}^{\mathrm{protein}}\frac{B_{\text{DNA-protein}}}{V_{\mathrm{nuc}}^2}}_{\text{DNA-protein}} + \underbrace{n_{\mathrm{nuc}}^{\mathrm{poly}}n_{\mathrm{nuc}}^{\mathrm{protein}}\frac{B_{\mathrm{nuc}}^{\text{poly-protein}}}{V_{\mathrm{nuc}}^2}}_{\text{polysome-protein}}. \quad \text{(S22)}$$

Similarly, taking the derivative of Eq. S20 with respect to V_{cyto} yields the osmotic pressure from the cytosol phase:

$$\Pi_{\mathrm{cyto}} = \underbrace{\frac{n_{\mathrm{cyto}}^{\mathrm{protein}}\left[1+\phi_{\mathrm{cyto}}^{\mathrm{protein}}+\left(\phi_{\mathrm{cyto}}^{\mathrm{protein}}\right)^2-\left(\phi_{\mathrm{cyto}}^{\mathrm{protein}}\right)^3\right]}{V_{\mathrm{cyto}}\left(1-\phi_{\mathrm{cyto}}^{\mathrm{protein}}\right)^3}}_{\text{protein}} + \underbrace{\frac{n_{\mathrm{cyto}}^{\mathrm{poly}}}{V_{\mathrm{cyto}}}\left[1+\left(\frac{\phi_{\mathrm{cyto}}^{\mathrm{poly}}}{0.69\phi_{\mathrm{cyto,ov}}}\right)^{1.309}\right]}_{\text{polysome}}$$
$$+ \underbrace{n_{\mathrm{cyto}}^{\mathrm{poly}}n_{\mathrm{cyto}}^{\mathrm{protein}}\frac{B_{\mathrm{cyto}}^{\text{poly-protein}}}{V_{\mathrm{cyto}}^2}}_{\text{polysome-protein}}. \quad \text{(S23)}$$

To understand the osmotic pressure exerted by crowders on the nucleoid, we use Eq. S22 and Eq. S23 to calculate the differences in partial osmotic pressure of crowder species between the two phases ($\Delta\Pi_{\mathrm{protein}}$, $\Delta\Pi_{\mathrm{poly}}$). Notice the usual definition of partial pressure is not informative for our system because of strong interactions present between species. To avoid ambiguity arising from the interaction term between polysome and protein crowders, we assigned equal contributions from this term to both the polysome and protein partial pressures. The resulting differences in partial pressures due to proteins and polysomes across

the phase boundary between the nucleoid and cytosol are given by

$$\Delta\Pi_{\text{protein}} = \frac{n_{\text{cyto}}^{\text{protein}}\left[1+\phi_{\text{cyto}}^{\text{protein}}+\left(\phi_{\text{cyto}}^{\text{protein}}\right)^2-\left(\phi_{\text{cyto}}^{\text{protein}}\right)^3\right]}{V_{\text{cyto}}\left(1-\phi_{\text{cyto}}^{\text{protein}}\right)^3} - \frac{n_{\text{nuc}}^{\text{protein}}\left[1+\phi_{\text{nuc}}^{\text{protein}}+\left(\phi_{\text{nuc}}^{\text{protein}}\right)^2-\left(\phi_{\text{nuc}}^{\text{protein}}\right)^3\right]}{V_{\text{nuc}}\left(1-\phi_{\text{nuc}}^{\text{protein}}\right)^3} - n_{\text{nuc}}^{\text{protein}}\frac{B_{\text{DNA-protein}}}{V_{\text{nuc}}^2} + 0.5\left(n_{\text{cyto}}^{\text{poly}}n_{\text{cyto}}^{\text{protein}}\frac{B_{\text{cyto}}^{\text{poly-protein}}}{V_{\text{cyto}}^2} - n_{\text{nuc}}^{\text{poly}}n_{\text{nuc}}^{\text{protein}}\frac{B_{\text{nuc}}^{\text{poly-protein}}}{V_{\text{nuc}}^2}\right) \text{ and} \tag{S24}$$

$$\Delta\Pi_{\text{poly}} = \frac{n_{\text{cyto}}^{\text{poly}}}{V_{\text{cyto}}}\left[1+\left(\frac{\phi_{\text{cyto}}^{\text{poly}}}{0.69\phi_{\text{cyto,ov}}}\right)^{1.309}\right] - \frac{n_{\text{nuc}}^{\text{poly}}}{V_{\text{nuc}}}\left[1+\left(\frac{\phi_{\text{nuc}}^{\text{poly}}}{0.69\phi_{\text{nuc,ov}}}\right)^{1.309}\right] - n_{\text{nuc}}^{\text{poly}}\frac{B_{\text{DNA-poly}}}{V_{\text{nuc}}^2} + 0.5\left(n_{\text{cyto}}^{\text{poly}}n_{\text{cyto}}^{\text{protein}}\frac{B_{\text{cyto}}^{\text{poly-protein}}}{V_{\text{cyto}}^2} - n_{\text{nuc}}^{\text{poly}}n_{\text{nuc}}^{\text{protein}}\frac{B_{\text{nuc}}^{\text{poly-protein}}}{V_{\text{nuc}}^2}\right). \tag{S25}$$

We calculate $\Delta\Pi_{\text{protein}}$ and $\Delta\Pi_{\text{poly}}$ at $T = 37$ °C following Eq. S24 and S25 and compare the results with the bulk stress in the DNA coil due to its self-energy ($\tau_{\text{DNA}} \equiv -\frac{\partial F_{\text{DNA}}}{\partial V_{\text{nuc}}} = k_B T\alpha g V_{\text{nuc,free}}^{\alpha}/V_{\text{nuc}}^{\alpha+1}$) in Fig. 2d in the main text.

Minimization of the free energy

We minimize the free energy F_{demix} with respect to V_{nuc}, $n_{\text{nuc}}^{\text{protein}}$, $n_{\text{nuc}}^{\text{poly}}$ and R_g^{poly} (the latter with possibly different values in the nucleoid and cytosol phases). The form of the free energy is rather complicated (Eq. S19, S20) and may contain many local minima. Different initial guesses for the parameters may trap any given minimization algorithm in different local minima. For the results we present in this paper, we used the Nelder-Mead algorithm (9) in the Scipy Python package. To ensure that a global free energy minimum is found, we set multiple initial guesses for the parameters and compare the resulting values of the free energy. We then pick the result that gives the lowest free energy as the solution. In the case where we vary the crowing conditions slightly, we then use this initial minimization result as the initial guess for the next crowding condition. Any jumps in the parameter values are scrutinized to ensure that they represent true phase transitions, rather than spurious results of the minimization procedure.

Including tracer particles

In order to study the partitioning of macromolecules between the nucleoid and cytosol phases we include spherical tracer particles of diameter $\boldsymbol{a_t}$ to our model. These particles are present in sufficiently dilute concentrations ($\boldsymbol{\phi}_{\max} \approx \mathbf{0.002}$) such that they do not affect nucleoid volume. The tracer particles are included via additional terms added to the free energy, given by

$$\boldsymbol{F}_{\text{tracer}} = \boldsymbol{F}_0 + \boldsymbol{F}_{\text{DNA-tracer}} + \boldsymbol{F}_{\text{poly-tracer}} + \boldsymbol{F}_{\text{protein-tracer}}, \tag{S26}$$

where the first term includes the ideal entropic and Carnahan-Starling terms for spherical particles. The last three terms represent the interaction between spherical tracers and the corresponding molecules in the subscripts, with $\boldsymbol{F}_{\text{poly-tracer}}$ following from Eq. S15 and $\boldsymbol{F}_{\text{protein-tracer}} = \boldsymbol{n}_{\text{protein}}\boldsymbol{n}_{\text{tracer}}\frac{\boldsymbol{\pi}(\boldsymbol{a_p}+\boldsymbol{a_t})^{\boldsymbol{3}}}{\boldsymbol{6V}}$ the excluded volume interaction between two spherical species. We use an interpolated excluded volume $\boldsymbol{B}_{\text{DNA-tracer}}$ to evaluate the DNA-crowder excluded volume interactions, which are given by

$$\boldsymbol{F}_{\text{DNA-tracer}} = \boldsymbol{n}_{\text{tracer}}\frac{\boldsymbol{B}_{\text{DNA-tracer}}}{\boldsymbol{V}}, \tag{S27}$$

where

$$B_{\text{DNA-tracer}} = f\left[\frac{1}{8}\pi L_{\text{DNA}}\sin(\delta)\,(d_s + a_t)^2 + N_s\frac{\pi}{6}(d_s + a_t)^3\right] + \frac{(1-f)}{4}\pi L_{\text{DNA}}(d_{\text{DNA}} + a_t)^2. \tag{S28}$$

This expression for $F_{\text{DNA-tracer}}$ combines Eq. 3 and Eq. 4 in the main text as we expect large tracers to interact with DNA supercoiling structure (just as the polysomes) and small tracers to behave like proteins, with exclusion only from the DNA double helix (see Fig. S7). The empirical extrapolation function f used to characterize the transition between the two excluded volume regimes is analogous to the one used for the polysome-protein interaction described above. The function is

$$f \equiv \frac{1}{2}\left[1 + \tanh\left(\frac{a_t - \lambda}{\xi_{\text{DNA}}}\right)\right], \tag{S29}$$

where the parameter $\boldsymbol{\lambda}$ is the length scale at which we transition between the two regimes. It would be natural to guess it relates to the size of the DNA supercoiling segment $\boldsymbol{d_s}$. Also, $\boldsymbol{\xi}_{\text{DNA}}$ is the characteristic width of the transition zone between the two regimes. In this study, we use $\boldsymbol{\xi}_{\text{DNA}} = \mathbf{5}$ nm. We then minimize Eq. S26 with respect to the tracer number within the nucleoid to estimate the portion of tracers

being excluded from nucleoid (Fig. 5 in the main text). The effect of different $\boldsymbol{\xi_{DNA}}$ and $\boldsymbol{\lambda}$ on the partitioning of macromolecules between the nucleoid and cytosol phases is displayed in Fig. S8. The value of $\boldsymbol{\xi_{DNA}}$ determines how fast the DNA-tracer interaction transits from one regime to the other one. Therefore, we see the exclusion behavior of tracers from the nucleoid phase changes more drastically with smaller $\boldsymbol{\xi_{DNA}}$, as shown in Fig. S8a. Other than this effect, we found both $\boldsymbol{\xi_{DNA}}$ and $\boldsymbol{\lambda}$ have a minor overall influence on macromolecule partitioning in our model. It is also worth mentioning that the precise shape of the interpolation function only matters in determining the exclusion between DNA and macromolecular crowders with sizes between approximately $\mathbf{5}$ and $\mathbf{50}$ nm. In calculating nucleoid compaction curves, where we only include protein and polysome crowders, we have $\boldsymbol{f \approx 1}$ for polysomes and $\boldsymbol{f \approx 4 \times 10^{-5}}$ for proteins. Therefore, both crowders are away from the interpolation region.

Modeling the effect of rifampicin treatment at different growth rates

To model the growth rate dependence of nucleoid expansion under polysome dissociation, we must consider how the growth rate modifies a set of parameters including the polysome and protein numbers, the amount of DNA in the cell, and the cell volume. In the following subsections, we enumerate these parameters and identify the growth-rate dependence using a combination of literature results and experimental measurements. These dependencies are then used to calculate the phase diagrams in Fig. 4 of the main text. Note that these dependencies are based on measurements at 37 °C.

1) Cell volume

The cell volume is known to increase exponentially with the growth rate, μ, as $V = \mathrm{V_0} e^{\beta \mu}$ where β is constant (the nutrient-imposed bacterial growth law) (10), or equivalently $V = \mathrm{V_0} 2^{\beta/\mathrm{T_D}}$, where $T_D = \ln 2 \,/ \mu$ is the doubling time. For specific numbers, we relied on fitting our data with this function to experimental data from Ref. (11), extrapolating the later from values at 28 °C to 37 °C (SI Fig. S6a, SI Table S3), yielding $V_0 = 0.43\ \mu\mathrm{m}^3$ and $\beta = 47$ min.

2) Polysome numbers

The available data is pertinent for the ribosomal RNA (rRNA) mass per 10^9 cells (12). We then used the measured weight of ribosome ~ 4270.5 kDa (13) to convert the data from mass per cell to ribosome number per cell. For simplicity, we assume all rRNA are part of polysomes and each polysome consists of 10 ribosomes. This estimate somewhat overcounts the polysome numbers because only about 85% of rRNA is present in polysomes (12). We next fit these data points as a function of T_D using a power law

form as shown in Fig S5b. The power law function is multiplied by a factor 0.93 such that the polysome number at $T_D = 60$ min matches the value $n_{\mathrm{poly}} = 600$, found from fitting our model to experimental data, as shown in Fig. 1c of the main text.

3) The average amount of DNA per cell

We estimate the average amount of DNA as a function of the cell doubling time T_D using the following formula derived by Cooper and Helmstetter (14):

$$G_{\mathrm{avg}} = \frac{T_D}{C \ln 2}\left(2^{(C+D)/T_D} - 2^{D/T_D}\right), \tag{S30}$$

where G_{avg} is the average amount of DNA per cell in genome equivalents. The absolute amount of DNA is therefore G_{avg} multiplied by 4.6 Mb. We also have the parameter $C = 40$ min, which is the time between initiation and termination of chromosome replication. The parameter $D = 20$ min is the period between termination of a round of replication and the subsequent cell division. A plot of G_{avg} as a function of T_D is displayed in Fig. S6c. One can see that the amount of DNA increases dramatically for fast growth rates ($T_D \sim 20$ min.). This has important consequences for the parameters of our model.

4) The volume of free nucleoid volume $V_{\mathrm{nuc,free}}$

As the amount of DNA increases with the growth rate, we must modify our model parameters as a function of the growth rate. The length of the chromosomal DNA L_{DNA} and the number of DNA supercoiling segments N_s are expected to both grow linearly with G_{avg}. The volume of the nucleoid (DNA) in the absence of the cellular confinement, $V_{\mathrm{nuc,free}}$, should also change with T_D. Consider a chromosomal DNA polymer with a radius of gyration R_g^{DNA}. The volume occupied by the DNA can be estimated as

$$V_{\mathrm{nuc,free}} \sim \left(R_g^{\mathrm{DNA}}\right)^3 \sim \left(b_{\mathrm{DNA}} N_{\mathrm{DNA}}^{\nu}\right)^3, \tag{S31}$$

where b_{DNA} is the Kuhn length of the DNA polymer, N_{DNA} is the number of monomers (polymerization index), and ν is the Flory exponent (1). Since N_{DNA} should grow linearly with G_{avg}, $V_{\mathrm{nuc,free}}$ increases with the growth rate as $V_{\mathrm{nuc,free}} \propto G_{\mathrm{avg}}^{3\nu}$. In the DNA self-interaction (Eq. 2 in the main text) and as discussed above, ν is related to α via $\alpha \approx 1/(3\nu - 1)$. The value of $\alpha \approx 0.85$ is determined by fitting the compaction curve measurement. We can use the corresponding value $\nu \approx 0.73$ to estimate $V_{\mathrm{nuc,free}}$ for different growth conditions using Eq. (S31).

5) Protein numbers

The cytosolic protein crowder number is difficult to estimate as a large fraction of the total proteins is not

responsible for crowding and is instead bound to DNA, is a part of cell envelopes, is used in the construction of the ribosomes, etc. Indeed, only about a quarter of the total proteins can be considered cytosolic protein crowders (15). Overall, the total protein concentration in the cell has been reported to decrease slightly with increasing growth rate, as can be seen in SI Fig. S2H in (16), for example. We may expect a similar result for the cytosolic protein crowders, but it is unclear whether the different kinds of protein all increase and decrease in proportion to the total protein number as a function of growth rate. We therefore treated the number of cytosolic crowders as a free parameter of the model (x-axis of the phase diagrams in Fig. 4 of the main text) and explored how changing the protein numbers influences the nucleoid structure. Fitting to experimental data in Fig. 1c in the main text yielded protein numbers of 2.3×10^5 for slow growing cells of volume 0.7 μm^3.

Replacing the polysomes with 30S and 50S ribosomal subunits for the rifampicin treated cells

We assume that there are 10 translating ribosomes in one polysome ($\boldsymbol{N_{\mathrm{ribo}} = 10}$). After the rifampicin treatment, each translating ribosome breaks into one 30S and one 50S ribosomal subunit. 30S and 50S shell volumes have been estimated to be 1.3×10^3 nm^3 and 2.3×10^3 nm^3 , respectively (17). Treating these particles as spheres yields effective radii 6.8 nm and 8.2 nm, respectively. In the light of other uncertainties of the model, we neglect the size differences of the subunits and consider both to be of the same size with a diameter of 16 nm.

List of model assumptions

- The model does not include non-equilibrium effects on the nucleoid such as those arising from transcription and ribosomal dynamics during translation. The effects of co-transcriptional translation and transertion (coupled co-transcriptional translation and membrane insertion (18)) are also not considered. Note that we do not need to consider non-equilibrium effects arising from DNA replication because the experiments we are describing with our theory (5,11) measure cells with no ongoing DNA replication.
- The polysomes are treated within the framework of the Flory model. This model assumes no spacing between ribosome monomers and has a simplified description of the polymer elasticity and conformational entropy. We also do not take into account the energy-driven kinetic effects arising from the assembly of ribosomal subunits to polysomes and dissociation of ribosomes back

to their subunits.

- The soluble proteins are modeled as monodisperse hard spheres with diameter $a_p = 5$ nm.
- In estimating the excluded volume interactions between DNA and crowders, DNA is treated as a cylinder for the small crowders (proteins) and a uniform chain of supercoils for the large crowders (polysomes). Other larger putative superstructures that might arise from supercoil ordering are not considered. The extrapolation of the excluded volume interaction between DNA and crowders between two limiting size regimes is assumed to be sigmoidal (SI Eq. S28, S29).
- The supercoiled segments of DNA are assumed to be uniformly distributed throughout the chromosome and we assume no supercoil branching. The diameter of supercoiling segments has no direct experimental measurement. So, we estimate the supercoil diameter, $d_s \approx 30$ nm, via the persistence length and superhelical pitch angle of DNA (see Method in the main text for detail).
- Both 30S and 50S ribosomal subunits are assumed to be spherical particles of approximately the same diameter ≈ 16 nm (see SI text above for details). Their actual structure is more similar to a hemisphere shape.
- For the phase separation, no additional cost to forming interfaces between different phases in the model is assumed. As such, we do not consider the free energy cost of any spatial gradients in the various component concentrations.
- We assume a spherical cell for simplicity as our free energy only depends on the volumes of the nucleoid and cytosol phases. The model is compared to the spherocylindrical geometry of *E. coli*.
- We assume that the sole effect of rifampicin is the dissociation of ribosomes. Other potential effects arising from inhibition of transcription are neglected.

SI Figures

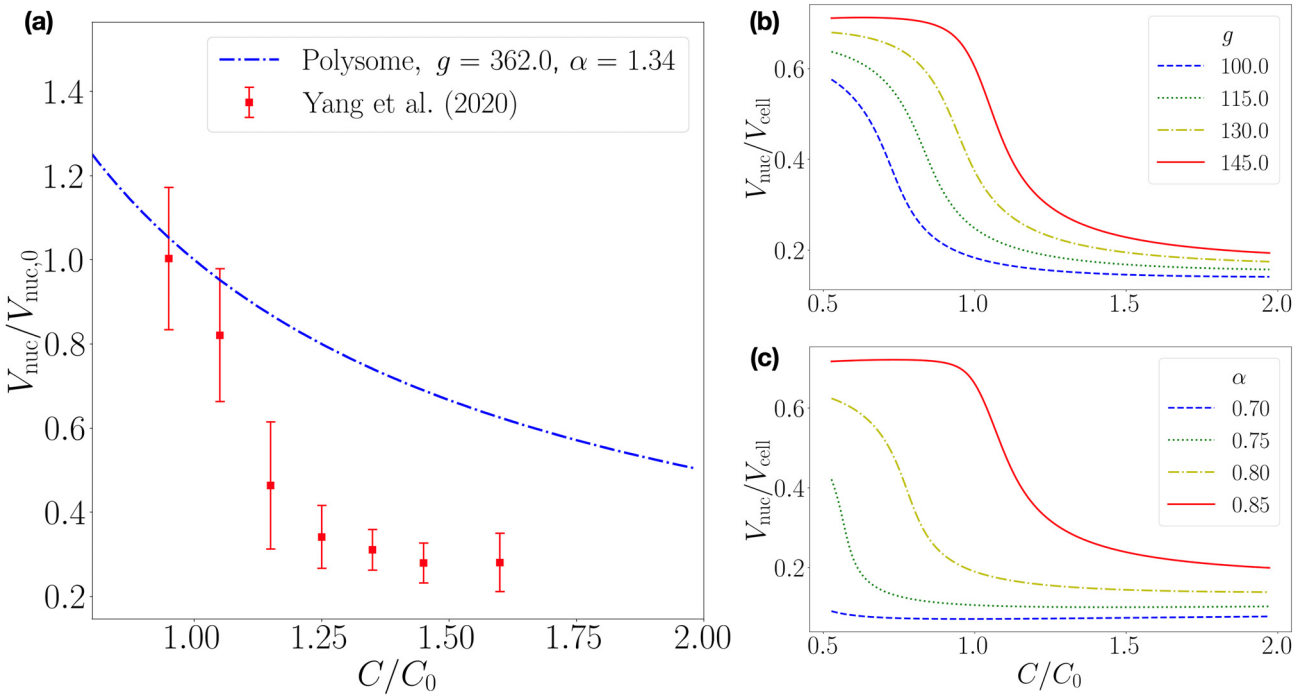

Figure S1: The effect of g and α to the nucleoid volume. (a) Using the g and α values from *in vitro* experiment (19) to fit the nucleoid compaction curves from the osmotic shock experiment (11). The nucleoid volume is scaled by the nucleoid volume $V_{\mathrm{nuc},0}$ at the physiological condition and each crowder concentration is scaled by their concentration at the physiological condition C_0. Note $C/C_0 = V_{\mathrm{cell},0}/V_{\mathrm{cell}}$ is the same for both crowder species. (b) The ratio of the nucleoid volume to cell volume as a function of C/C_0 for different g values. The other parameters of the model are that from Fig. 1c in the main text ($\alpha \approx 0.85$, $n_{\mathrm{poly},0} \approx 600$ and $n_{\mathrm{protein},0} \approx 2.3 \times 10^5$). (c) The ratio of the nucleoid volume to cell volume as a function of C/C_0 for different α values. The other parameters of the model are those from Fig. 1c in the main text ($g \approx 145.0$, $n_{\mathrm{poly},0} \approx 600$ and $n_{\mathrm{protein},0} \approx 2.3 \times 10^5$)

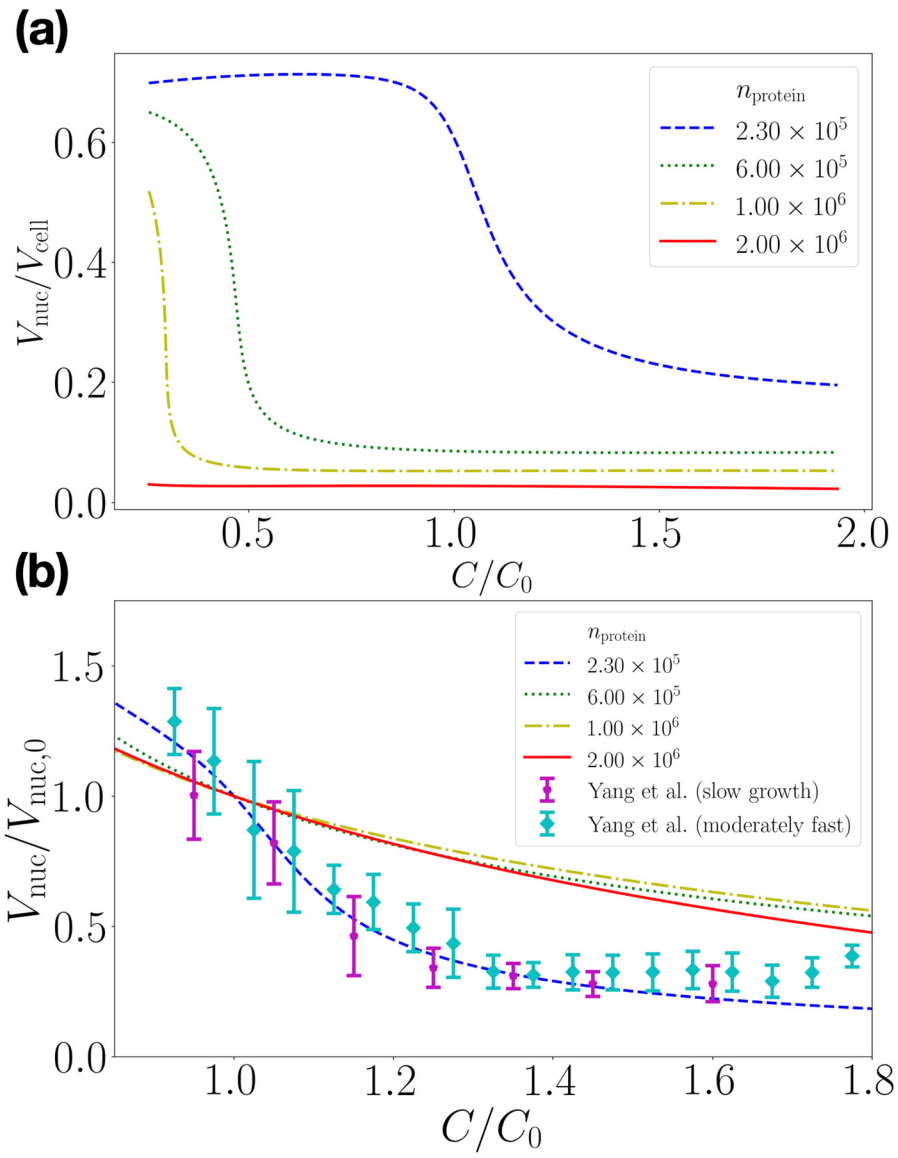

Figure S2: The compaction of nucleoid for higher soluble protein numbers. Each crowder concentration is scaled by their concentration at the physiological condition C_0. Note $C/C_0 = V_{\text{cell},0}/V_{\text{cell}}$ is the same for both crowder species. The number of polysomes is fixed for all curves ($n_{\text{poly}} = 600$). (a) The ratio of the nucleoid volume to cell volume as a function of C/C_0 for different soluble protein number n_{poly}. (b) Scaling the nucleoid volume by the nucleoid volume $V_{\text{nuc},0}$ at the physiological condition. The experimental data from osmotic shock measurements from (11) at slow and moderately fast growth conditions (SI Table S3) shown by magenta and blue points, respectively.

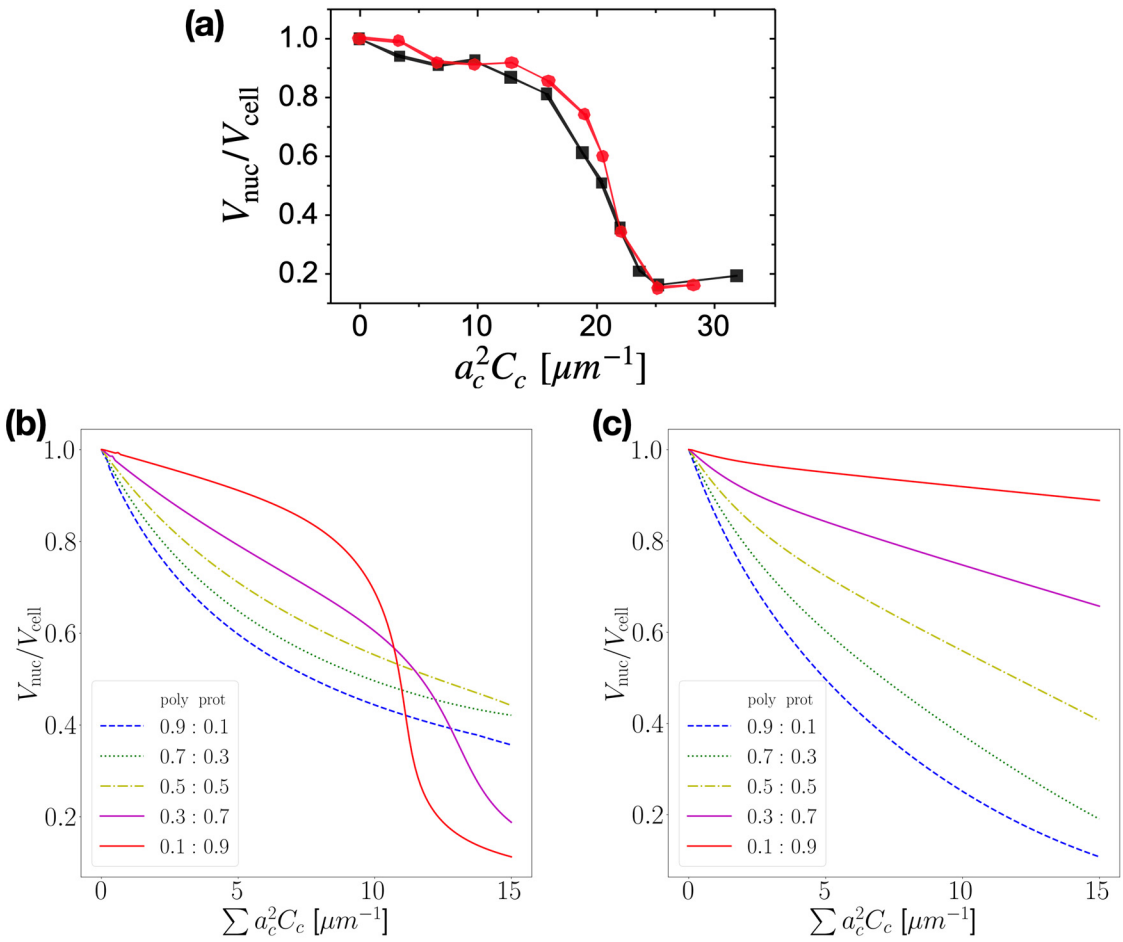

Figure S3: The scaling properties of $V_{\mathrm{nuc}}/V_{\mathrm{cell}}$ curves from our model differ from those of molecular dynamics modeling. Kim *et al.* (20) found that normalized nucleoid size curves collapse to each other at different crowder compositions if plotted against a quantity $\sum a_{c,i}^2 C_{c,i}$ where a_c is the diameter of crowder species i and $C_{c,i}$ is their number density. This finding was confirmed by Yang *et al.* (11). (a) Curves from molecular dynamics modeling from Yang *et al.* for two different crowder sizes (red - $a_c = 20$ nm, black - $a_c = 40$ nm). (b) $V_{\mathrm{nuc}}/V_{\mathrm{cell}}$ vs $\sum a_{c,i}^2 C_{c,i}$ from our model for different ratio of proteins to polysomes in the cell. The sum has one term for polysomes and another term for proteins. The ratios are defined by contribution of the species to the sum $\sum a_{c,i}^2 C_{c,i}$. For instance, 0.1 for polysomes (solid red line) means that $a_{c,\mathrm{poly}}^2 C_{c,\mathrm{poly}} = 0.1 \sum a_{c,i}^2 C_{c,i}$. (c) The same curves as in (b) but calculated for a model where the excluded volume between the polysomes and DNA neglects the supercoiled structure of DNA.

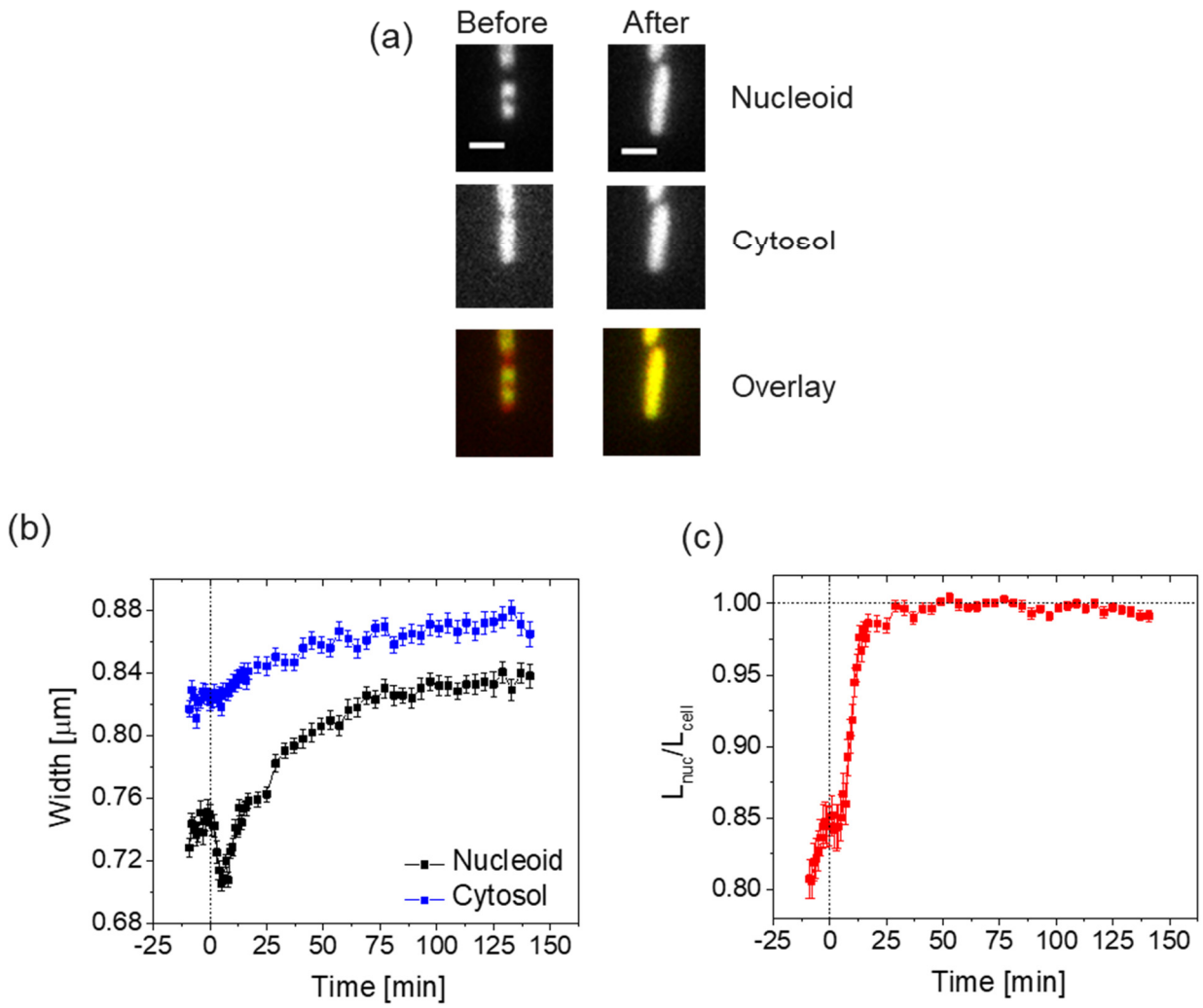

Figure S4: Nucleoid expansion under the rifampicin treatment for *E. coli* MG1655 cells grown in EZ-Rich medium supplemented with 0.2% glucose. (a) Images of a representative cell before and after treatment with 300 μg/ml rifampicin. The nucleoid is labelled by HupA-mNeonGreen and cytosol by tag-RFP-T fluorescent labels. Scale bar corresponds to 2 μm. (b) The width of the whole cytosol (black line) and the nucleoids (blue) for a cell population ($N = 72$) before and during the rifampicin treatment. The treatment starts at time zero. The initial decrease in nucleoid width has been assigned to the disruption of the transertion linkages (11,21). Interestingly, we find that the cell width also increases upon the rifampicin treatment. Error bars represent std error for the cell population. (c) Ratio of nucleoid length to the length of the whole cytosol for the same cell population. The details of the measurement and analysis can be found in (11).

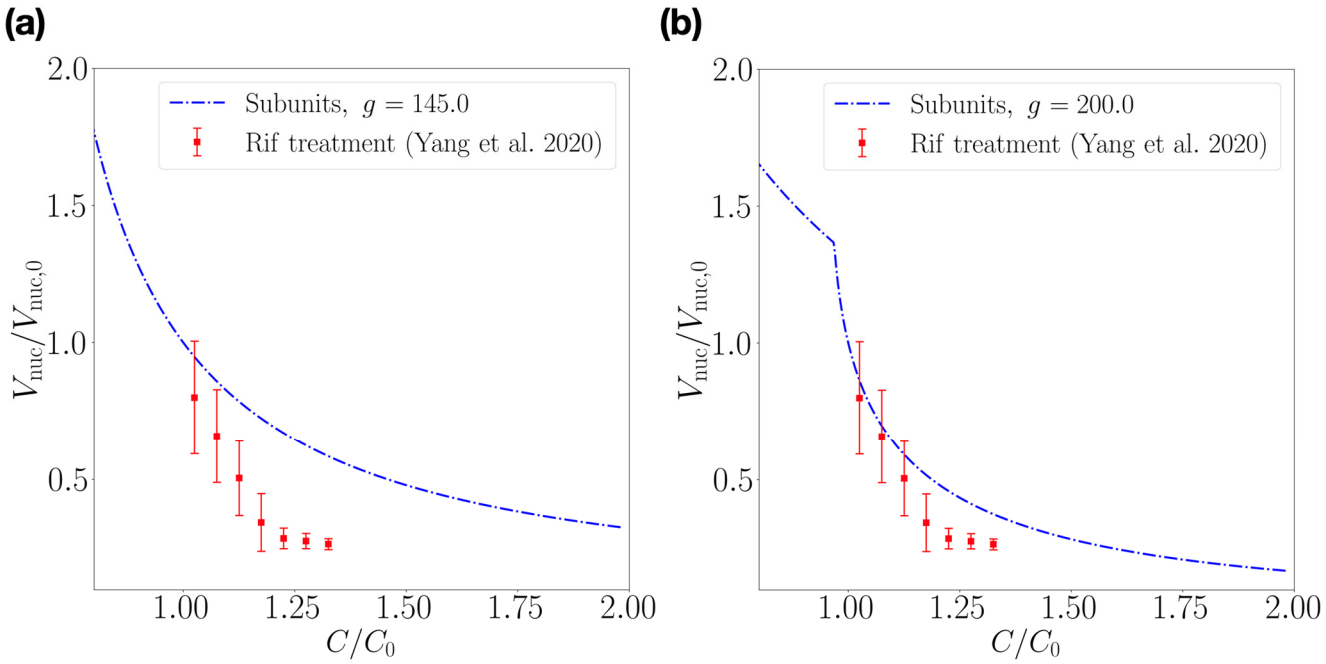

Figure S5: Fitting the nucleoid compaction curves of rifampicin treated cells from (11) to our model. (a) In the model a polysome are replaced by ten 30S and ten 50 subunits, each with a diameter of 16 nm. The excluded volume for these subunits follows the interpolation formula (Eq. S28, SI Fig. S7). All other parameters of the model are the same as in Fig. 1c of the main text ($\alpha = 0.85, g = 145, n_{\mathrm{poly}} = 600, n_{\mathrm{protein}} = 2.3 \times 10^5$). The model prediction is shown by a blue dash-dot line. (b) The best fit value for this model when g is optimized. The best fit value $g = 200$.

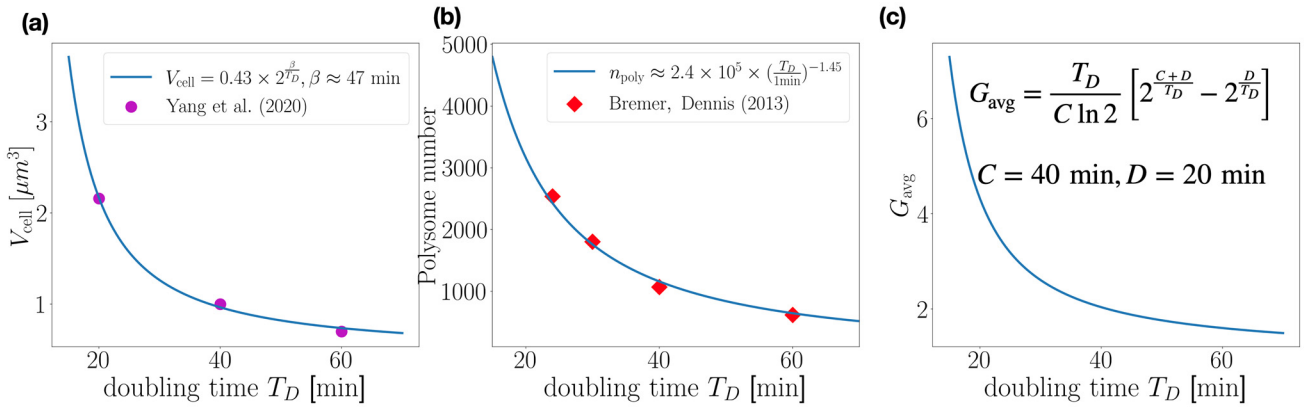

Figure S6: The average cell volume, polysome numbers, and DNA amount at different doubling times for *E. coli* cells. (a) The average cell volume versus doubling time. The data is based on measurements by Yang et al. (11). The doubling times at 28 °C are interpolated to those at 37 °C based on Table S3. The cell volume is assumed to be the same at both temperatures. The solid line is fit to the data by $V_{\text{cell}} = 0.43 \cdot 2^{\beta/T_D}$, $\beta \approx 47$ min. (b) Polysome numbers as a function of doubling times based on measured RNA mass in the cells (12). For the details of how the polysome numbers are calculated from RNA mass (see SI Text). The data is from measurement at 37 °C. The data is fitted to a power law $n_{\text{poly}} = 2.4 \times 10^5 \times \left(\frac{T_D}{1\text{min}}\right)^{-1.45}$ (blue solid curve). The scaled polysome numbers is displayed as the orange dashed line, which is used model the growth rate dependence of nucleoid expansion under polysome dissociation (see SI Text). (c) The average DNA amount in the cell as a function of doubling time. The amount is expressed in genome units (4.6 Mb). The amount is calculated based on formula by Cooper and Helmstetter (14).

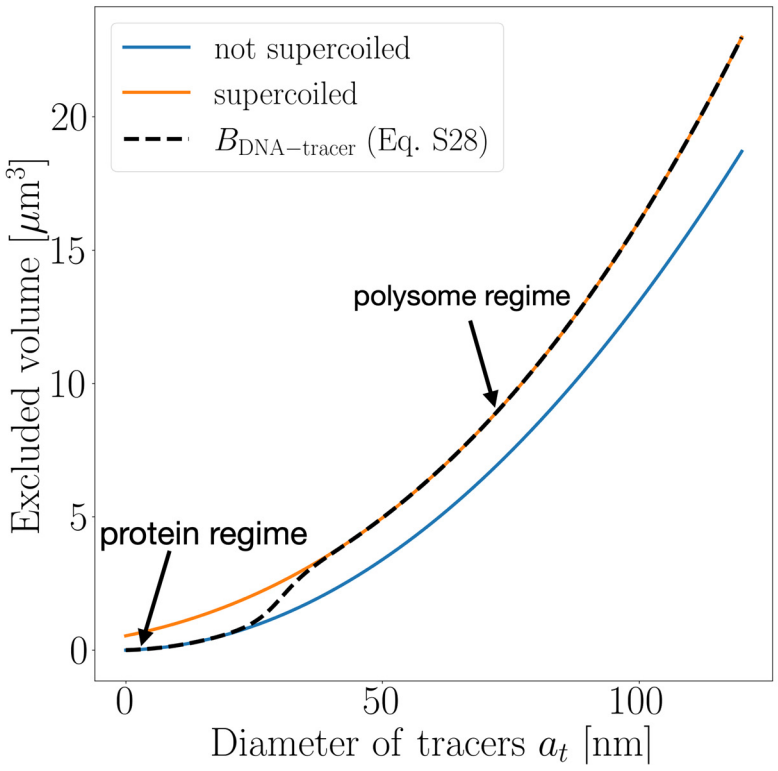

Figure S7: The first-order virial coefficient for DNA-tracer interaction, $B_{\mathrm{DNA\text{-}tracer}}$, as a function of the diameter of crowders (a_t). Blue line – the excluded volume between straight DNA (not supercoiled) and spherical hard-sphere molecules (Eq. 3 in the main text). Orange line - the excluded volume between DNA supercoils and spherical hard-sphere molecules (Eq. 4 in the main text). The dashed line interpolates between the two curves using the empirical extrapolation function f (Eq. S29). Here we set the characteristic width $\xi_{\mathrm{DNA}} = 5$ nm and $\lambda = 30$ nm. The typical diameters of proteins and polysomes are schematically indicated.

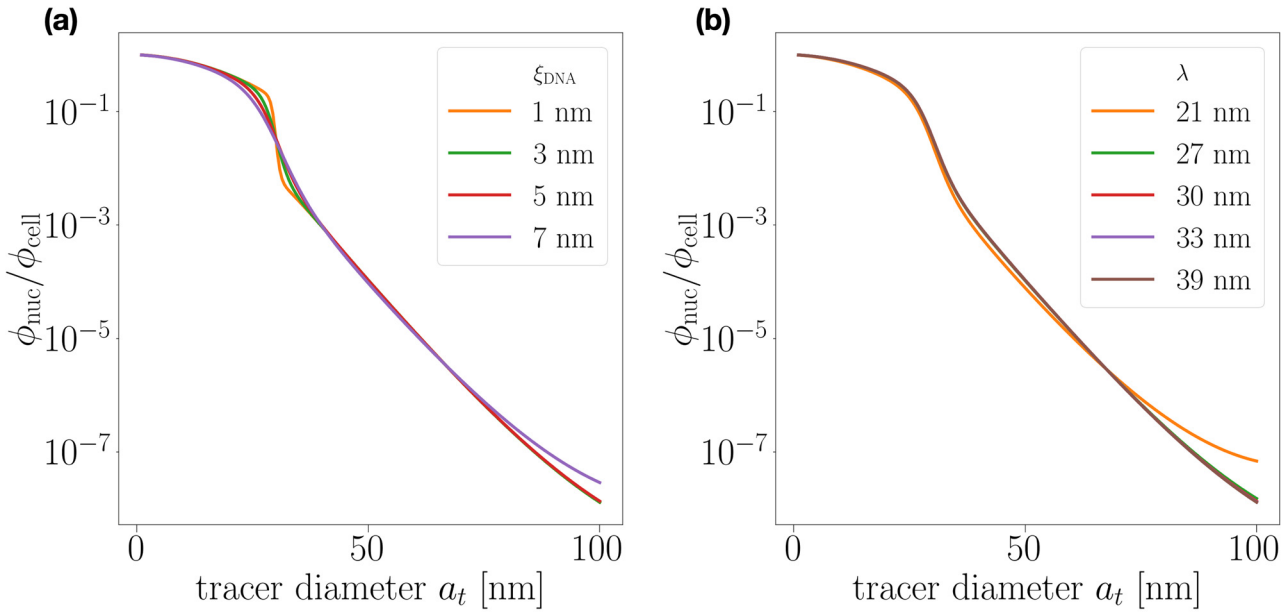

Figure S8: The dependence of the partitioning of macromolecules between the nucleoid and cytosol phases on their linear dimensions for different interpolation functions f (SI Eq. S28, Fig. S7), which governs the excluded volume between tracer and DNA in the free energy model. (a) The effect of varying the width of the interpolation function, ξ_{DNA}. λ is fixed at 30 nm in this panel. (b) The effect of varying the center of the interpolation region, λ. Note $\lambda = 30$ nm corresponds to the diameter of the supercoiling segments d_s. ξ_{DNA} is fixed at 5 nm in this panel.

SI Tables

Table S1: Notations

	Symbol	Unit	Ref. Value* slow growth
The cell volume	V_{cell}	μm^3	
The cell volume at the physiological condition	$V_{\text{cell,0}}$	μm^3	~ 0.7 (11)
The pre-factor in DNA self-interaction (Eq. 2 in the main text)	g		145-200, 362 (19)
The exponent in DNA self-interaction (Eq. 2 in the main text)	α		~ 0.85, 1.34 (19)
Diameter of tracer particles	a_t	nm	1-100
Volume of the nucleoid	V_{nuc}	μm^3	
Radius of gyration of polysome	R_g^{poly}	nm	~ 35
Number of polysomes	n_{poly}		~ 620 (12)
Volume fraction of polysomes	ϕ_{poly}		~ 0.07
Number of proteins	n_{protein}		~ 2.3×10^5
Volume fraction of proteins	ϕ_{protein}		~ 0.02
Volume of the nucleoid at the physiological condition	$V_{\text{nuc,0}}$	μm^3	~ 0.38 (11)
Concentration of polysome	C_{poly}	$1/\mu m^3$	
Concentration of protein	C_{protein}	$1/\mu m^3$	
Osmotic pressure exerted by polysomes to DNA	Π_{poly}	pascal (Pa)	
Osmotic pressure exerted by proteins to DNA	Π_{protein}	pascal (Pa)	
Doubling time of the cell	T_D	min	~ 60 (11)
Growth rate of the cell	μ	1/hr	~ 0.69 (11)
Concentration of crowders at the physiological condition	$C_{\text{c,0}}$	$1/\mu m^3$	
Overlap volume fraction of polysomes	ϕ_{ov}		~ 1.9
First-order virial coefficient	B	μm^3	
Inverse of fractal dimension (Flory exponent)	ν		~ 0.73 (for DNA)

Average amount of DNA per cell in genome equivalent	G_{avg}		~ 1.67
Bulk stress of DNA	τ_{DNA}	pascal (Pa)	
Bulk modulus of DNA	κ_{DNA}	pascal (Pa)	
Compressibility of DNA	β_{DNA}	1/Pa	
Free energy in units with $\boldsymbol{k_B T \equiv 1}$	F		

*All listed values are based on this work unless otherwise specified

Table S2: Model parameters

	Symbol	Value	Comment/ Ref
Diameter of the DNA supercoiling segment	d_s	30 nm	$d_s = P\cos\delta$
Length of the chromosomal DNA per genome equivalent	L_{DNA}	1.6 mm	4.6 Mb
Diameter of double helix DNA	d_{DNA}	2 nm	
Plectoneme opening angle (pitch angle)	δ	52°	(22)
Diameter of ribosome	a_{ribo}	20 nm	(23)
Diameter of protein	a_p	5 nm	
Number of DNA supercoiling segments per genome equivalent	N_s	6700	(23), (24)
Number of ribosomes per polysome	N_{ribo}	10	(23)
Volume of the isolated nucleoid	$V_{\text{nuc, free}}$	27 μm^3	(19)
Persistence length of plectoneme	P	50 nm	(22)
Characteristic width in interpolation formula for DNA-crowder interaction	ξ_{DNA}	5 nm	
Length scale dividing the two regimes in interpolation formula for DNA-crowder interaction	λ	30 nm	
Characteristic width in interpolation formula for polysome-protein interaction	ξ_{poly}	10 nm	

Table S3. Extrapolation of doubling times at 28 °C to doubling times at 37 °C. The first two columns from the left are the growth media and doubling times from measurements by Yang et al (11) at 28 °C. The corresponding double times at 37 C is from (12). The growth media in both datasets is the same except that EZRich glucose the data in (11) is considered to yield the same growth rate as LB+glucose medium in (12). The growth rate in the 4th column is calculated as $\mu = \ln 2/T_D$. $\langle V_{cell} \rangle$ is the average cell volume based on data in (11).

Growth Medium	T_D **(28 °C)** [min]	**Growth Rate (28 °C)** [1/hr]	T_D **(37 °C)** [min]	**Growth Rate (37 °C)** [1/hr]	$\langle V_{cell} \rangle$ [μm^3]
Slow: M9 glycerol	225±103	0.18±0.08	60	0.69	0.7
Moderately fast: M9 glucose+casamino acids	95±24	0.43±0.11	40	1.04	1.0
Fast: EZRich+glucose	53±7	0.78±0.11	20	2.08	2.2

References

1. Rubinstein, M. and R. Colby. (2003) *Polymer Physics*. Oxford University Press, New York.
2. Hansen-Goos, H. and R. Roth. 2006. A new generalization of the Carnahan-Starling equation of state to additive mixtures of hard spheres. J Chem Phys 124: 154506.
3. Wiggins, P.A., K.C. Cheveralls, J.S. Martin, R. Lintner and J. Kondev. 2010. Strong intranucleoid interactions organize the *Escherichia coli* chromosome into a nucleoid filament. Proc. Natl. Acad. Sci. U. S. A. 107: 4991-4995.
4. Benza, V.G., B. Bassetti, K.D. Dorfman, V.F. Scolari, K. Bromek, P. Cicuta and M.C. Lagomarsino. 2012. Physical descriptions of the bacterial nucleoid at large scales, and their biological implications. Reports on Progress in Physics 75: 076602.
5. Xiang, Y.J., I.V. Surovtsev, Y.J. Chang, S.K. Govers, B.R. Parry, J. Liu and C. Jacobs-Wagner. 2021. Interconnecting solvent quality, transcription, and chromosome folding in *Escherichia coli*. Cell 184: 3626-3642.
6. Fleer, G.J., A.M. Skvortsov and R. Tuinier. 2007. A simple relation for the concentration dependence of osmotic pressure and depletion thickness in polymer solutions. Macromol Theor Simul 16: 531-540.
7. Schäfer, L. (1999) *Excluded volume effects in polymer solutions, as explained by the renormalization group*. Springer, Berlin.
8. Minton, A.P. 2005. Models for excluded volume interaction between an unfolded protein and rigid macromolecular cosolutes: macromolecular crowding and protein stability revisited. Biophys. J. 88: 971-985.
9. Gao, F. and L. Han. 2012. Implementing the Nelder-Mead simplex algorithm with adaptive parameters. Computational Optimization and Applications 51: 259-277.
10. Schaechter, M., O. Maaloe and N.O. Kjeldgaard. 1958. Dependency on medium and temperature of cell size and chemical composition during balanced growth of *Salmonella Typhimurium*. Journal of General Microbiology 19: 592-606.
11. Yang, D., J. Männik, S.T. Retterer and J. Männik. 2020. The effects of polydisperse crowders on the compaction of the *Escherichia coli* nucleoid. Mol Microbiol 113: 1022-1037.
12. Bremer, H. and P. Dennis. 2008. Modulation of chemical composition and other parameters of the cell at different exponential growth rates. EcoSal Plus,doi: doi:10.1128/ecosal.5.2.3.
13. Noeske, J., M.R. Wasserman, D.S. Terry, R.B. Altman, S.C. Blanchard and J.H. Cate. 2015. High-resolution structure of the Escherichia coli ribosome. Nature structural & molecular biology 22: 336-341.
14. Cooper, S. and C.E. Helmstetter. 1968. Chromosome replication and division cycle of *Escherichia coli* B/r. Journal of Molecular Biology 31: 519-540.
15. Li, G.W., D. Burkhardt, C. Gross and J.S. Weissman. 2014. Quantifying absolute protein synthesis rates reveals principles underlying allocation of cellular resources. Cell 157: 624-635.
16. Balakrishnan, R., M. Mori, I. Segota, Z.G. Zhang, R. Aebersold, C. Ludwig and T. Hwa. 2022. Principles of gene regulation quantitatively connect DNA to RNA and proteins in bacteria. Science 378: 1066.
17. Voss, N.R. (2007) *Geometric Studies of RNA and Ribosomes, and Ribosome Crystallization*. Yale University.
18. Woldringh, C.L. 2002. The role of co-transcriptional translation and protein translocation (transertion) in bacterial chromosome segregation. Mol. Microbiol. 45: 17-29.

19. Cunha, S., C.L. Woldringh and T. Odijk. 2001. Polymer-mediated compaction and internal dynamics of isolated *Escherichia coli* nucleoids. J. Struct. Biol. 136: 53-66.

20. Kim, J., C. Jeon, H. Jeong, Y. Jung and B.Y. Ha. 2015. A polymer in a crowded and confined space: effects of crowder size and poly-dispersity. Soft Matter 11: 1877-1888.

21. Bakshi, S., H. Choi, J. Mondal and J.C. Weisshaar. 2014. Time-dependent effects of transcription- and translation-halting drugs on the spatial distributions of the *Escherichia coli* chromosome and ribosomes. Mol. Microbiol. 94: 871-887.

22. Boles, T.C., J.H. White and N.R. Cozzarelli. 1990. Structure of plectonemically supercoiled DNA. Journal of Molecular Biology 213: 931-951.

23. Mondal, J., B.P. Bratton, Y.J. Li, A. Yethiraj and J.C. Weisshaar. 2011. Entropy-based mechanism of ribosome-nucleoid segregation in *E. coli* cells. Biophys. J. 100: 2605-2613.

24. Miangolarra, A.M., S.H.J. Li, J.F. Joanny, N.S. Wingreen and M. Castellana. 2021. Steric interactions and out-of-equilibrium processes control the internal organization of bacteria. Proc. Natl. Acad. Sci. U. S. A. 118: e2106014118.